General Disclaimer

One or more of the Following Statements may affect this Document

- This document has been reproduced from the best copy furnished by the organizational source. It is being released in the interest of making available as much information as possible.

- This document may contain data, which exceeds the sheet parameters. It was furnished in this condition by the organizational source and is the best copy available.

- This document may contain tone-on-tone or color graphs, charts and/or pictures, which have been reproduced in black and white.

- This document is paginated as submitted by the original source.

- Portions of this document are not fully legible due to the historical nature of some of the material. However, it is the best reproduction available from the original submission.

The Pennsylvania State University
The Graduate School
Department of Meteorology

Determination of Surface Characteristics and Energy Budget Over an Urban-Rural Area Using Satellite Data and a Boundary Layer Model

A Thesis in

Meteorology

by

Joseph Kent Dodd

Submitted in Partial Fulfillment
of the Requirements
for the Degree of

Master of Science

August 1979

The Pennsylvania State University

The Graduate School

Department of Meteorology

Determination of Surface Characteristics and Energy Budget Over an Urban-Rural Area Using Satellite Data and a Boundary Layer Model

A Thesis in

Meteorology

by

Joseph Kent Dodd

Submitted in Partial Fulfillment
of the Requirements
for the Degree of

Master of Science

August 1979

The signatories below indicate that they have read and approved the thesis of Joseph Kent Dodd:

Date of Signature:	Signatories:
June 29, 1979	Toby R. Carlson, Associate Professor of Meteorology, Thesis Advisor
[illegible]	Hans A. Panofsky, Evan Pugh Professor of Atmospheric Sciences
July 8, 1979	Alfred K. Blackadar, Head of the Department of Meteorology

ABSTRACT

A flexible analysis system has been developed which combines high resolution satellite-derived radiometric ground temperature information with output from a numerical model of the boundary layer to infer the spatial variation of thermal inertia (P), moisture availability (M), and the surface energy budget.

The system has been applied to the urban areas of Los Angeles and St. Louis for which observations of ground temperature near the times of maximum and minimum were available from the polar orbiting Heat Capacity Mapping Mission (HCMM) satellite which has a horizontal resolution of .5 kilometers. From this data false-color-enhanced (RAMTEK) images or computer-produced contoured fields of surface temperature may be derived. Further analysis uses the temperature data with output from the model to infer the spatial distributions of thermal inertia, moisture availability, and surface heat and moisture flux across both cities.

The mapping of these quantities over the St. Louis and Los Angeles regions revealed the marked influence which reduced evaporation exercises in forcing the positive daytime temperature anomaly over cities. Both urban centers possessed maxima of heat flux and minima of moisture flux whereas forested or grassy areas nearby displayed quite the opposite trend. The nighttime temperature anomaly was found to be relatively weak as the distributions of P were unexpectedly ill-defined.

TABLE OF CONTENTS

	Page
ABSTRACT	iii
LIST OF TABLES	v
LIST OF FIGURES	vi
ACKNOWLEDGEMENTS	viii
1.0 INTRODUCTION	1
1.1 Past Research in Urban Microclimates	1
1.2 Statement of the Problem	7
1.3 Purpose of the Thesis	8
2.0 METHOD OF ANALYSIS	10
2.1 The Model	10
2.2 Data Reduction and Analysis	27
2.3 Coordination of Model Output and Satellite Data	33
3.0 RESULTS	41
3.1 Background	41
3.2 Los Angeles May 30 and 31, 1978	50
3.2.1 May 31 Daytime Temperatures, T_D	50
3.2.2 May 30 Nighttime Temperatures, T_N	52
3.2.3 May 30-31 Moisture Availability, M	54
3.2.4 May 30-31 Thermal Inertia, P	56
3.2.5 May 31 Surface Heat Flux, H_o	58
3.2.6 May 31 Surface Evaporative Flux, E_o	60
3.3 St. Louis June 9 and 10, 1978	60
3.3.1 June 10 Daytime Temperatures, T_D	62
3.3.2 June 9 Nighttime Temperatures, T_N	64
3.3.3 June 9-10 Moisture Availability, M	66
3.3.4 June 9-10 Thermal Inertia, P	68
3.3.5 June 10 Surface Heat Flux, H_o	68
3.3.6 June 10, Surface Evaporative Flux, E_o	71
3.4 Summary of Results	71
4.0 CONCLUSIONS AND SUGGESTIONS FOR FUTURE RESEARCH	81
REFERENCES	85

LIST OF TABLES

Table		Page
1	HCMM satellite orbital and radiometer characteristics.	46
2	Model input parameters for case studies.	48

LIST OF FIGURES

Figure		Page
1	Basic structure of model.	11
2	Flow chart of model solution sequence from time t_o to $t_o + \Delta t$	18
3	Basic structure of nocturnal component of model . .	22
4	Schematic of initial wind and temperature profiles for the nocturnal component of model.	25
5	Schematic diagram of the satellite data processing procedure	29
6	Example of daytime surface temperature mapping across Los Angeles for May 31, 1978	30
7	Example of RAMTEK graphics for daytime surface temperatures across Los Angeles, May 31, 1978 . . .	31
8	Flow diagram for inferring surface parameters . . .	35
9	Schematic representation of TOPO subset area. . . .	36
10	Schematic illustration of incrementation process and day-night temperature arrays.	38
11	A population density map of the Los Angeles area with a letter key marking areas of interest referenced in the text.	43
12	A road map of St. Louis and vicinity with a letter key marking areas of interest referenced in the text.	45
13	Los Angeles, May 31, 1978 daytime surface temperature analysis.	51
14	Los Angeles, May 30, 1978 nighttime surface temperature analysis.	53
15	Los Angeles moisture availability analysis.	55
16	Los Angeles thermal inertia analysis.	57
17	Los Angeles surface sensible heat flux (÷ 10) at 2:00 P.M. (R_N = 630 W/m^2)	59
18	Los Angeles surface moisture flux (÷ 10) at 2:00 P.M. (R_N = 630 W/m^2)	61

LIST OF FIGURES (Continued)

Figure		Page
19	St. Louis, June 10, 1978 daytime surface temperature analysis.	63
20	St. Louis, June 9, 1978 nighttime surface temperature analysis.	65
21	St. Louis moisture availability analysis.	67
22	St. Louis thermal inertia analysis.	69
23	St. Louis surface sensible heat flux (÷ 10) at 2:00 P.M. (R_N = 640 W/m^2)	70
24	St. Louis surface moisture flux (÷ 10) at 2:00 P.M. (R_N = 640 W/m^2)	72
25	Enlargement of unsmoothed surface heat flux analysis over downtown St. Louis at 2:00 P.M. . .	75
26	Daytime evolution of surface heat and moisture flux and net radiation from model simulation for St. Louis urban site (M = .175, P = .035)	78
27	Daytime evolution of surface heat and moisture flux and net radiation from model simulation for St. Louis rural site (M = .5, P = .035)	80

ACKNOWLEDGEMENTS

I wish to thank Dr. Toby Carlson for his guidance and encouragement throughout the course of this research and Jim Cooper for his programming support which aided in the data analysis.

This study was supported by the Environmental Protection Agency (EPA) under Contract R-805 640020 and the National Aeronautical and Space Administration (NASA) Contract NAS-5-24264. Thanks is also extended to The Pennsylvania State University Office of Remote Sensing of Earth Resources for the use of RAMTEK computer graphics. Finally, computations for the thesis were performed on an IBM 370/168 at The Pennsylvania State University.

1.0 INTRODUCTION

1.1 Past Research in Urban Microclimates

Observation of urban temperature anomalies dates back to the work of Howard (1833) who documented temperature elevations over London of 2°F. Contemporary studies by Duckworth and Sandberg (1954), Landsberg (1956), and Oke (1968) show urban-rural temperature differences of up to 10°F with the greatest urban temperature elevations occurring on clear, calm winter nights. While the elevation of ground and air temperature in urban environments has received considerable attention, other more recent investigations have led to an assessment of the effect of cities on precipitation. Changnon (1969) was one of the first to present evidence of significant urban enhancement of rainfall. Huff and Vogel (1978) analyzed summer rainfall from the Metropolitan Meteorological Experiment (METROMEX) network of 225 recording rain gauges distributed in and surrounding St. Louis and found 10-30% increases in precipitation in and downwind of the city during the season of convective rainfall. From the same project, Changnon (1978) found very significant (locally to 300%) increases in thunderstorm duration and intensity, hail events, and rainfall both in and downstream from St. Louis. Braham and Wilson (1977) also observed urban enhancement of the frequency and duration of tall convective cloud echoes over St. Louis during METROMEX.

It has been suggested that the alteration of the surface energy budget as a result of the heteorogeneous composition of the substrate, unique to urbanized areas, is responsible for important effects of cities upon the environment. Ching, Clark, and Godowitch (1978) showed that over urban areas variability in the sensible heat flux depends upon the

land use, specifically the thermal characteristics of the substrate (diffusivity and conductivity). Yap and Oke (1974) used the eddy correlation technique to measure urban sensible heat transfer over Vancouver, B.C. and concluded that vertical flux convergence at night in the surface layer is responsible for the heat island. They also observed that the partitioning of the nocturnal energy budget exhibited a unique urban character. Landsberg and Maisel (1972) have proposed that the urban canopy maintains high values of thermal conductivity and heat capacity. They also showed that the net radiation is smaller by day and larger by night in cities.

Detection of urban anomalies is not restricted to in situ measurements. In the last decade extensive use has been made of aircraft and satellite measurements in identifying the way in which cities alter their environments. Rao (1972) was the first to show how satellites could be used to study the radiometric properties of urban areas. Carlson and Augustine (1977) demonstrated how high resolution satellite data could be used in the spatial representation of thermal signatures in cities. Matson et al. (1978) were able to detect over 50 urban heat islands from thermal infrared images of the mid-western and northeastern United States generated by the NOAA5 satellite.

Numerical models of urban boundary layers have also been able to successfully reproduce the gross effects of urban structure upon temperature and surface fluxes and, more importantly, have firmly identified the substrate characteristics which force the urban anomalies. Estoque (1963) was one of the first to create a physical model with analytic representations for air and surface temperature, moisture, and wind simulated numerically and integrated on a computer. Tag (1968)

further extended this work to study the effect of environmental factors (pollution, roughness) on the urban heat island in particular. Independent of these efforts, Myrup (1969) was the first to develop a numerical energy budget model to study the urban heat island exclusively. He assumed a neutral boundary layer, equating the eddy diffusivities for momentum and heat, but assumed an unrealistically large surface layer depth of 300 m over which the fluxes remain constant. Myrup simulated the urban rural features by changing the thermal conductivity and diffusivity, roughness length, and evaporation potential. The dominant parameters which determined the magnitude of the urban heat island effect were found to be evaporation, which was reduced in the city during the day, while the thermal properties of the soil caused the temperature to be elevated at night. Outcalt (1972) extended Myrup's model, improving the solar radiation computation and other physical representations. Comparison of model results with field data showed very good agreement.

Nappo (1972), in another numerical study of the urban heat island effect, performed extensive sensitivity tests to show that the dominant parameters influencing temperature anomalies are surface roughness, moisture, and soil characteristics. As with Myrup, the surface temperature is calculated using the energy balance equation at the ground surface. In a similar study, Sasamori (1970) used his boundary layer model to show that the division of the energy balance into sensible and latent heat is distinctly dependent on soil wetness. Through the application of a model developed by Pandolfo, Atwater (1972) showed that the urban heat island is a result of physical changes in surface characteristics produced by urbanization, and not pollution of the

atmosphere. He was able to produce urban-rural air temperature contrasts in excess of 5°F by simply changing the soil diffusivity and heat capacity. The reduction of moisture availability was also identified as a causative mechanism. Atwater (1975) reached similar conclusions in extending this work to two and three dimensions employing conservation equations for wind, temperature, moisture, and pollution concentration. In this way the inclusion of advection produced a thermal plume of positive temperature anomaly both over and downwind of the urban area simulated.

Zdunkowski and Trask (1971) applied a radiative-conductive model to examine the evolution of the nocturnal surface temperature as a function of different soil types. The soils (rocky, quartz sand, sandy clay, and humus) were all uniquely specified by their density, specific heat, and diffusivity. The strongest nocturnal cooling was identified with the sandy soil, due to its poor conductivity, while the rocky soil remained relatively warm at night as enthalpy stored in the substrate is readily conducted to the surface.

All of the above investigations have contributed significantly to the understanding of horizontal and vertical variation of temperature and heat flux over and across an urban area. In addition, the urban heat island has been identified as responsible for major weather modifications on the short mesoscale and the dominant parameters which determine these alterations of cities upon climate have been isolated and explained. Little attention, however, has been focused on the problem of inferring the values of the parameters themselves through the coordination of model application and actual observation. In principle, it is reasonable to suppose that temperature information (which usually

is one of the predicted parameters) might be used in conjunction with a numerical boundary layer model to solve for the substrate parameters which determine the thermal response of the ground to the solar forcing.

In a unique study using a variation of this approach, Dabberdt and Davis (1974) evaluated the effective surface geophysical features with specific aim to determine the thermal and evaporative descriptors of a variety of land use types through the application of Lettau's climatonomy theory to in situ and remote observations. They used harmonic analysis on the observations of solar radiation and temperature to infer the secondary responses as a function of surface type. As an extension of their work they saw the possibility of evaluating the spatial variability of surface parameters such as thermal inertia across an area with a wide range of land uses and cover. The methodology of analysis would require high-resolution surface temperature data in space and time with a rather laborious application of harmonic analysis in the solution sequence. Although their results were encouraging no further research has modified or extended this approach.

Carlson and Boland (1978) proposed a numerical-graphical method for inferring the thermal inertia and moisture availability of the surface by analysis of pairs of day-night observations in which these parameters were varied systematically in a one-dimensional boundary layer model and the simulated temperatures matched with satellite derived temperatures. The Carlson-Boland method removes some of the ambiguity in determining the substrate characteristics by inverting the model. Their method requires in situ measurements of surface temperature to obtain a solution for the substrate parameters, thus necessitating the use of high-resolution satellite information to better define

the thermal fields. For example, the surface temperature may be defined as the average in the top 1 mm of the soil or that of the air in contact with the ground. The correct definition of surface temperature is not obvious and measurements of this type are rarely available, certainly not with the spatial density needed for analysis on urban scales. Such surface temperatures, even if they were available, would represent only a small area and have significant variability over short distances in heterogeneous terrain. On the other hand, a satellite measures the effective surface radiometric temperature with resolutions of .25 to 1 km^2 (HCMM and NOAA) and thus integrates the complex surface response over an area rather than sampling at a specific point. Such area-averaged temperatures will represent the spatially averaged thermal response to the partitioning of the available solar energy. This partitioning is determined by a set of substrate properties which apply to scales over which the observations are averaged. For high-resolution satellites, the resolution is highly appropriate to the urban mesoscale.

In situ measurements of temperature and heat flux can provide information appropriate only to a limited scale such as a particular parking lot, building, or field. Clearly, such limited site-specific measurements do not offer much help in inferring the spatial variation in the bulk characteristics of the surface parameters over an urban domain. Carlson and Boland proposed that satellite derived day-night temperature pairs define (through application of the model) the appropriate values of the surface parameters which govern this particular thermal response on an urban scale.

1.2 Statement of the Problem

It is obvious that much attention has been focused on the meso-scale alteration of climate through the rearrangement of the surface energy budget caused by urbanization. The process of replacing natural vegetation and soils with a heterogeneous urban landscape results in significant changes in the substrate characteristics and has had demonstrated effects on the microclimates of cities. Typically, the complex mixture of roads, houses, buildings, and parking lots which comprise the urban fabric is able to store the incident solar energy during the day more efficiently than adjoining rural areas and conduct this stored heat back to the ground-atmosphere interface more readily at night. Also, evaporation within cities is severely restricted in comparison with adjacent rural environments. Other parameters such as surface roughness and albedo have spatial inhomogenities that combine to produce the temperature elevation typical of cities which has been labeled the urban heat island.

Numerical modeling of the urban boundary layer is dependent on a knowledge of the surface heat flux and is complicated by a cluttered surface fabric which can only be described empirically. Thus, surface layer models are composed of a combination of empirical parameters and approximate relationships between temperature, the fluxes of sensible and latent heat, and solar plus terrestrial radiation. Values of substrate parameters such as thermal diffusivity, soil wetness, etc., which are required to determine the surface temperature response in such models, are customarily estimated from published tables in combination with land use maps (e.g., Sellers, 1965) but close inspection of urban surface temperatures (Augustine, 1978) indicates that such

parameters may have significant and complex variability. Observational studies (Oke, 1968 and Chandler, 1965) indicate large temperature and heat flux variations across cities.

Little work beyond that of Carlson and Boland has been done in measuring or inferring the urban-rural variation of basic surface parameters which govern the partitioning of the surface energy balance. Such information is crucial before one can be able to model correctly the influence of the surface fabric upon the microclimates of cities and thereby allow one to forecast the dispersion of pollutants and the effect that modifications of the surface fabric have upon the weather. As the populations of industralized nations continue their strong migration to urban centers, understanding how cities can alter their environment becomes increasingly relevant.

1.3 Purpose of the Thesis

This research involves the application of a one-dimensional boundary layer model developed by Carlson and Boland (1978) coupled with high resolution measurements of surface temperature made by satellite to infer the substrate parameters, thermal inertia and moisture availability, and the surface energy budget over urban areas. These surface parameters, to be defined later, have been shown by Boland (1977) and others to be the dominant ones in determining the thermodynamic response of the ground and atmosphere to the solar forcing over urban areas. The integration of satellite information with the numerical model is a unique feature of the analysis; the method to be described will be used to map the thermal and moisture properties over two major urban centers, St. Louis and Los Angeles. Further, the

surface energy balance will also be derived from this method, allowing for the first time an analysis of the substrate parameters and of the surface energy budget over a large urban area. Although the aim is to assess patterns over these urban areas, the method described has general applicability to other types of surfaces.

2.0 METHOD OF ANALYSIS

2.1 The Model

The first component necessary in the analysis procedure which will be pursued is a one-dimensional numerical model of the boundary layer developed by Carlson and Boland (1978) which allows one to calculate surface temperature and the energy flux components at the surface. The model represents the physics of the response of the ground to the solar forcing by using Monin-Obukov theory with an implicit K-type parameterization for the eddy fluxes in the surface layer. The primary forcing is the net radiation; but the partitioning of the energy balance into the ground heat flux and the latent and sensible heat fluxes into the atmosphere is determined by the substrate and atmospheric variables. Solutions are obtained as successive equilibrium states of the energy balance controlled by similarity theory in the surface layer and the temperature diffusion equation in the soil. Typically, the model is integrated to simulate a complete diurnal cycle over which the terrain parameters and the temperature at the bottom of the substrate slab (1m below the surface) are held constant. Advection and anthropogenic heat sources have been neglected in the current investigation.

A schematic view of the model dimensions is presented in Figure 1. The soil slab is one meter deep and divided into four layers. The surface air layer depth is fixed at 50 meters with a 1 cm transition layer at the earth's surface which contains both molecular and eddy heat conduction.[1] Within this transitional sublayer the fluxes of moisture and heat are assumed to be independent of the stability.

---

[1]The exact depth of the transition layer is inconsequential insofar as the surface temperature determination is concerned.

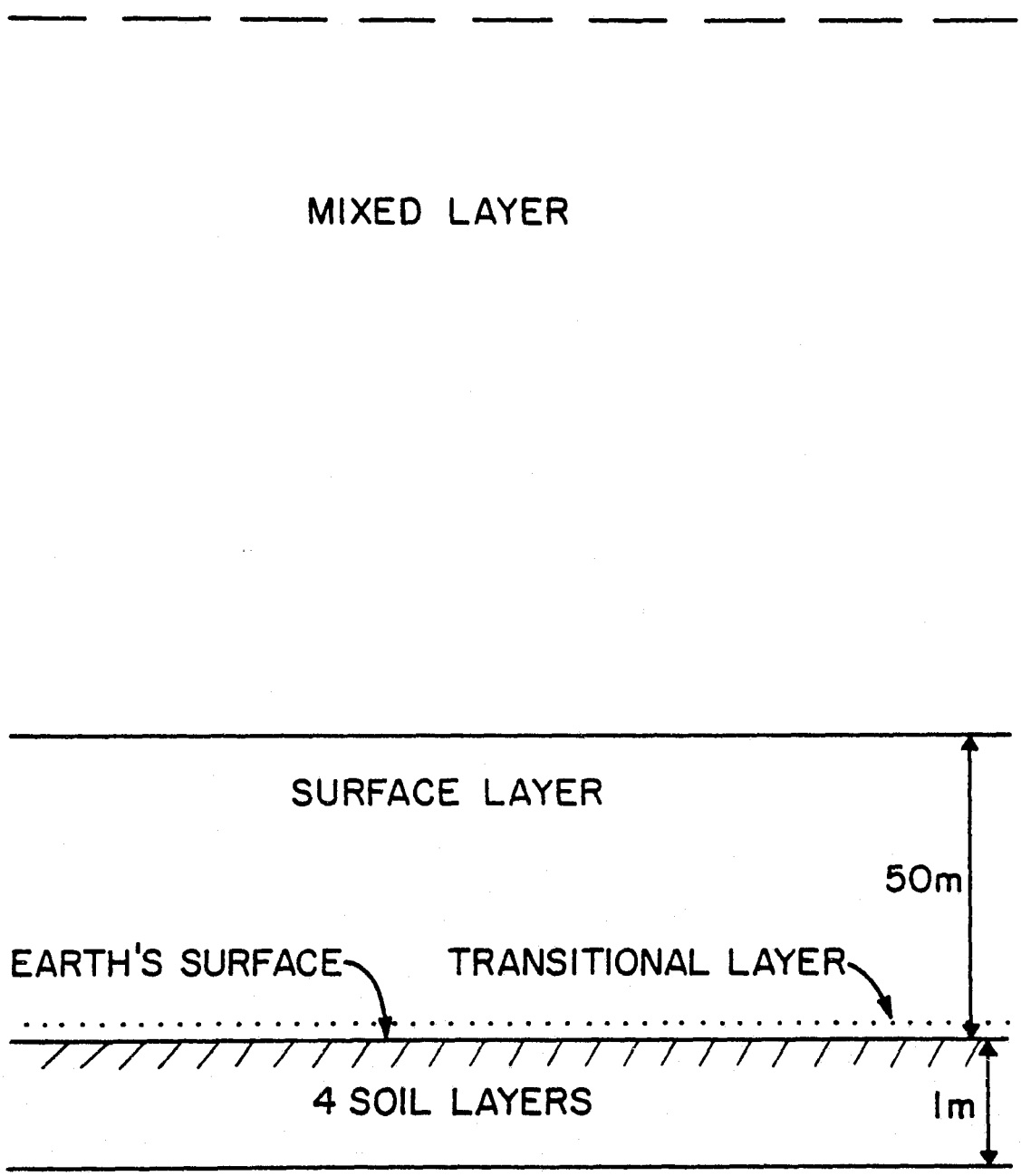

Figure 1. Basic structure of model.

A well-mixed layer is represented in bulk form above the surface layer and its depth, H, is governed by a formulation presented by Tennekes (1973) in which H grows throughout the day as a result of the surface heat flux from below and entrainment of air with a higher potential temperature from above. The atmosphere above the surface layer is represented differently at night and part of the present work has involved incorporating in the model a modification of the nocturnal boundary layer component which will be given in detail later.

The solution sequence begins with the net radiation given by the surface energy balance

$$R_N = G_o + H_o + E_o \tag{1}$$

where G_o, H_o, and E_o represent the heat flux into the ground, the sensible heat flux into the atmosphere, and the latent heat flux into the atmosphere. All quantities are positive when directed away from the surface. The net radiation is actually calculated from the radiative fluxes at the surface

$$R_N = S + F_d - F_u \tag{2}$$

where S is the solar flux at the surface and F_d and F_u are the upward and downward terrestrial fluxes respectively. Total down-dwelling irradiance absorbed at the surface, S, is calculated from a one-layer radiative transfer model described by Augustine (1977). S is a function of solar geometry, atmospheric transmission coefficients, and ground

albedo, A_o, determined as

$$S = S^* (1 - A_o)/(1 - XA_o) \tag{3}$$

where S* and X are general transmission relations containing the solar constant and coefficients for dust, water vapor, air molecules, ozone, and clouds. The upward and downward directed fluxes of longwave terrestrial radiation are given as

$$F_u = \varepsilon_g \sigma T_g^4 \tag{4}$$

$$F_d = \varepsilon_A(w) \sigma T_A^4 \tag{5}$$

where σ is the Boltzman constant and ε_g and $\varepsilon_A(w)$ are the emissivities for the ground and atmosphere. Sellers (1965) gives values of ε_g between .9 and 1 while Monteith (1961) has presented a formula which allows the calculation of ε_A as a function of the precipitable water, w.

The surface fluxes of sensible and latent heat are parameterized in terms of eddy and molecular diffusivities as

$$H_o = - (C_s + \rho c_p K_H) \frac{\partial \theta}{\partial z} \tag{6}$$

$$E_o = - \left(\frac{L_E}{c_p} C_w + \rho L_E K_q\right) \frac{\partial q}{\partial z} \tag{7}$$

where C_s and C_w are the molecular diffusivities for heat and water vapor, q. L_E is the latent heat of vaporization and K_H and K_q are the eddy diffusivities for heat and water vapor, which are assumed to be

equal. The ground temperature and mixing ratio are derived by integrating eqs. 6 and 7 from Z=0 to the top of the surface layer, Z_A

$$\theta_o = T_o = \theta_A + H_o I/\rho c_p \tag{8}$$

$$q_o = q_A + E_o I/\rho c_p \tag{9}$$

where I is essentially the vertical integral of the inverse of the diffusivities

$$I = \int_o^{Z_A} \frac{dz}{(K_H + C_s/\rho c_p)} = I_1 + I_2 \tag{10}$$

This integral is calculated in two sections: from z=0 to Z_ℓ, the depth of the transitional layer over which molecular conduction dominates the transfer process, while from Z_ℓ to Z_a, C_s and C_w are assumed to be negligible compared with $(\rho c_p K_H)$; thus turbulent eddy conduction determines the exchange in evaluating the expression I_2. Substition of $ku_* z/\phi_h$ for K_H is made where u_* is given by

$$u_* = \bar{u}_A k / \int_{Z_o}^{Z_A} \frac{\phi_m(z)}{z}\, dz \tag{11}$$

and $\bar{u}_A$ is the wind speed at Z_A, k is von Karman's constant (.4), and Z_o is the roughness length. The functional forms for ϕ_H and ϕ_M have been given by Panofsky (1974) and the integrals I_2 and 11 have recently been solved by Benoit (1977) for the unstable case.

The evaporative flux at the surface is given as

$$E_o = \frac{\rho L_E}{I} M(q_{os} - q_o) \tag{12}$$

where q_{os} is the surface saturation mixing ratio, q_A is the mixing ratio at Z_A, and M is the moisture availability parameter described by Nappo (1974). Values of M range from 0 to 1 and represent a fraction of the potential evaporation rate for a saturated surface. As such, the factor M accounts for the reduction in the efficiency of evaporation due to the subsaturation of the surface. One might suspect that the moisture availability will display significant urban-rural differences. In the model M is held constant over the diurnal cycle and the evaporation is set to zero at night when $q_A > q_{os}$.

The ground heat flux is given by the standard conduction equation

$$G_o = \lambda(T_o - T_{-1})/\Delta z \tag{13}$$

where λ is the thermal conductivity of the substrate and T_{-1} is the temperature at the first soil level, a distance Δz (10 cm) below the surface. The transfer of heat through the soil is governed by the diffusion equation

$$\frac{\partial T}{\partial t} = \frac{\partial^2 T}{\partial z^2} \tag{14}$$

where κ is the thermal diffusivity of the substrate and is equivalent to λ/C_g, C_g being the ground heat capacity.

The diffusivity and conductivity may be combined to form a parameter called the thermal inertia, P, where

$$P = \lambda/\kappa^{1/2} \qquad \text{Units : } P\ (cal\ cm^{-2}\ K^{-1}\ sec^{-1/2}) \qquad (15)$$

is a measure of the rate of heat transfer at the interface between the ground and atmosphere. Sensitivity tests have shown that while model solutions depend on the value of P independently of the choices of λ and κ, the last two must not be chosen completely independent of one another. It was noticed that values of λ and κ cited in the literature appear to vary systematically for a wide variety of real materials. Accordingly, 20 pairs of λ and κ based on values reported in the Manual of Remote Sensing (1975) and by Sellers (1965) have been assembled to produce a regression equation whereby specification of P will determine uniquely a λ,κ pair. Thus, it was found that

$$\lambda = -.00013 + .0502P + 1.21P^2 \qquad (16)$$

$$\text{Units : } \lambda\ (cal\ cm^{-1}\ sec^{-1})$$

where

$$\kappa = \lambda^2/P^2 \qquad (17)$$

Equation 16 explains 91% of the variance of λ about P and provides an empirical result which, for most types of materials, realistically

represents the physical relationship of λ and κ to P. The regression equation 16 corresponds to a diverse range of soil types (pumice to quartzite). The essential value of equation 16 is that it permits specification of a single bulk property, P, in terms of λ or κ which are explicitly represented in the model.

Equations 8, 12, and 13 may be combined with the energy balance equation 11 to form an expression for the sensible heat flux at the surface

$$H_o = [R_N - f(\bar{u}_A)M(q_{os} - q_A) - A]/(1 + DI) \tag{18}$$

in which

$$A = \lambda(\Gamma Z_A + T_o - T_{-1})/\Delta z \tag{18a}$$

$$D = \lambda/\Delta z \rho c_p \tag{18b}$$

where Γ is the dry adiabatic lapse rate and $f(\bar{u}_A)$ is $(\rho L_E/I)$.

This series of equations is cycled through for convergence. One iteration per time step of four minutes has been found sufficient to insure accurate solutions. The flow chart in Figure 2 schematically traces the order of calculation, the sequence ending with the determination of the temperature profile in the soil at the next time step from which the model integration time is incremented and the cycle repeated. The temperature profile in the surface layer and substrate, as well as the surface radiative and turbulent energy fluxes, are all part of the solution set.

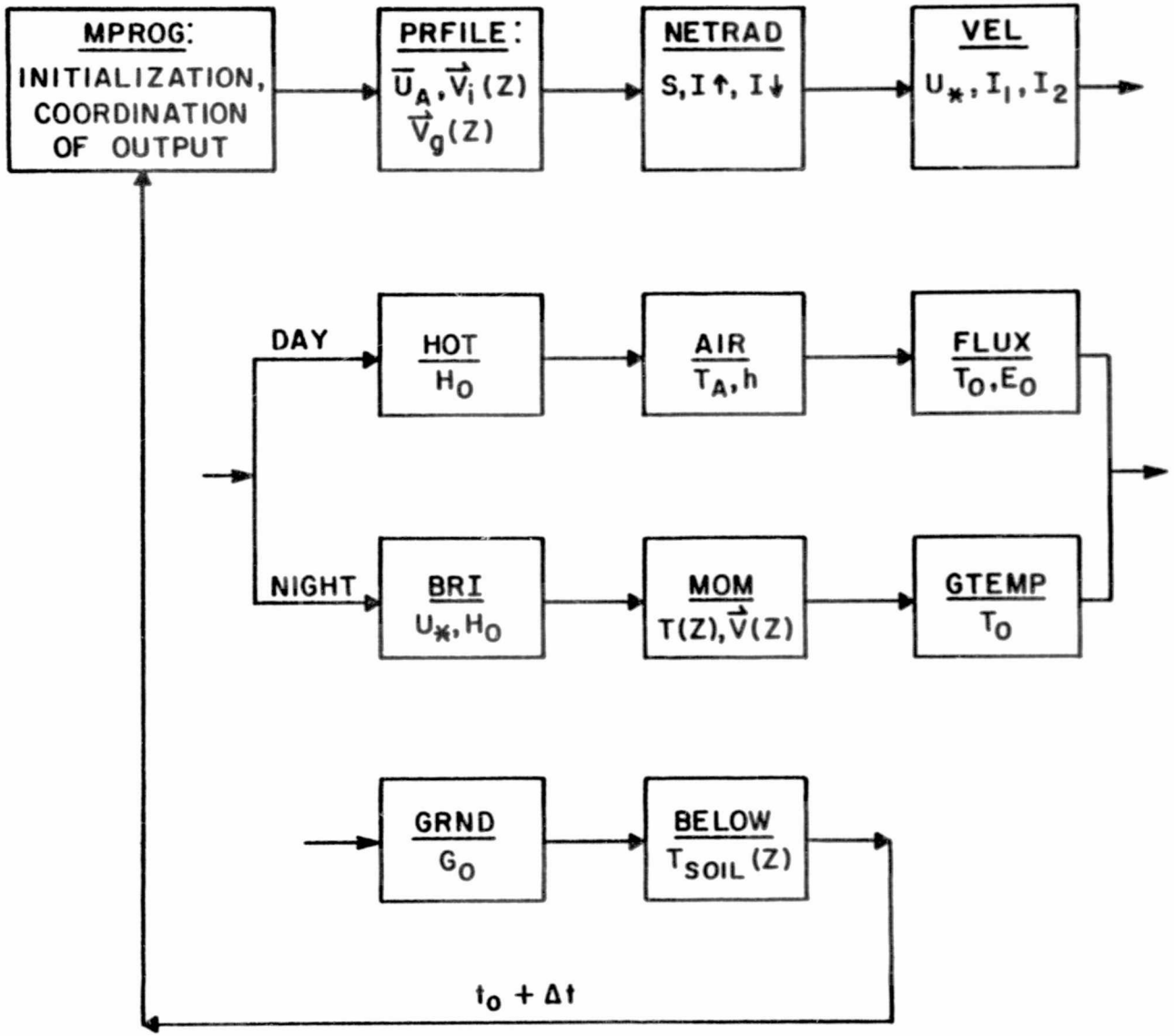

Figure 2. Flow chart of model solution sequence from time t_o to $t_o + \Delta t$.

The nighttime mode of calculation follows a different methodology as the physics driving the surface layer are quite dissimilar from the daytime. During the day the net radiation is the forcing mechanism and the heat flux component is a function of the moisture availability and thermal inertia. At this time the surface layer will be unstable and the heat flux will determine the stability; toward sunset the upward heat flux vanishes and the radiational cooling causes the ground temperature to decrease with time and subsequently the heat flux becomes passively dependent on the lapse rate near the ground. To account for this, a modified form of a scheme proposed by Blackadar (1976) has been incorporated into the model where the maintenance of turbulence at night is calculated as a function of the bulk Richardson number, B, in the surface layer. The value of B will determine the form of the profile equations and is given by

$$B = \frac{g}{\bar{\theta}} \frac{Z_A}{W_A^2} \left[(\theta_A - \theta_1) + T_* \ln \frac{Z_A}{Z_o} \right] \tag{19}$$

where g is the acceleration due to gravity, $\bar{\theta}$ is an average temperature in the surface layer, θ_A is the potential temperature at Z_A, and θ_1 is a "shelter" height temperature provided by a prognostic equation relating radiational convergence and turbulent flux convergence

$$\frac{\partial \theta_1}{\partial t} = A(\theta_{SO} - \theta_1) + B \frac{H_o}{\rho c_p Z_1} \tag{20}$$

in which A and B have been empirically determined as $8.3 \times 10^{-4} s^{-1}$ and 0.2 respectively. Monin-Obukov scaling is used to obtain T_*, u_*, and the surface heat flux, H_o. Thus,

$$T_* = (\theta_A - \theta_1)/(\ln Z_1/Z_A - \psi_h) \tag{21}$$

$$u_* = kW_A/(\ln Z_1/Z_o - \psi_m) \tag{22}$$

$$H_o = - k\rho c_p u_* T_* \tag{23}$$

where Z_o is the roughness length, ψ_h and ψ_m are the non-dimensional profiles for temperature and wind, the functional forms of which are dependent on stability, and W_A is the magnitude of the wind vector at a height Z_A (50 meters). The vertical profiles for temperature and wind are provided through the integration of the U, V momentum equations and the thermodynamic equation,

$$\frac{\partial U_i}{\partial t} = f(V_i - V_{gi}) + \frac{K_{mi+1}}{\Delta z^2}(U_{i+1} - U_i) - \frac{K_{mi}}{\Delta z^2}(U_i - U_{i-1}) \tag{24}$$

$$\frac{\partial V_i}{\partial t} = -f(U_i - U_{gi}) + \frac{K_{mi+1}}{\Delta z^2}(V_{i+1} - V_i) - \frac{K_{mi}}{\Delta z^2}(V_i - V_{i-1}) \tag{25}$$

$$\frac{\partial \theta_i}{\partial t} = \frac{K_{Hi+1}}{\Delta z^2}(\theta_{i+1} - \theta_i) - \frac{K_{Hi}}{\Delta z^2}(\theta_i - \theta_{i-1}) \tag{26}$$

where f is the Coriolis parameter and Δz is a layer depth of 50 meters. Advection has not been included in the model. The eddy exchange coefficients for momentum and heat, K_M and K_H, are assumed equal in the stable nocturnal boundary layer and are given by a form proposed by Mellor and Yamada (1974) using boundary layer data and 2nd order closure

$$K_i = \ell^2 S_i \left(\frac{Rc_i - R_i}{Rc_i}\right) \tag{27}$$

where,

$$S_i = [(U_i - U_{i-1})^2 + (V_i - V_{i-1})^2]^{1/2}/\Delta z \tag{28}$$

and ℓ scales as kz (taken to be 28m) in the surface layer. The local Richardson number is calculated as

$$R_i = \frac{g}{\bar{\theta}\Delta z} \frac{(\theta_i - \theta_{i-1})}{S_i^2} \tag{29}$$

while the critical Richardson number is calculated as a function of the geostrophic wind using an empirical result given by Vigeant (1978)

$$Rc_i = .5542\, e^{-[.2129(U_{gi}^2 + V_{gi}^2)^{1/2}]} + .2 \tag{30}$$

When the local Richardson number exceeds the critical value turbulent exchange will cease at that height and K is arbitrarily set equal to zero.

The lowest layer must be treated differently as there will be no turbulent exchange through the underlying surface. Accordingly, the last terms in equations 24-26 must be replaced by $\frac{-u_*^2 U_1}{W_A \Delta z}$, $\frac{-u_*^2 V_1}{W_A \Delta z}$, and $\frac{-H_o}{c_p \rho \Delta z}$ respectively.

The integration is performed over a 500 meter deep layer consisting of 10 equi-spaced intervals (i=1,10) 50 meters apart (Figure 3) and is begun in the late afternoon or evening when the surface heat flux has changed sign and the nocturnal mode of calculation in the surface

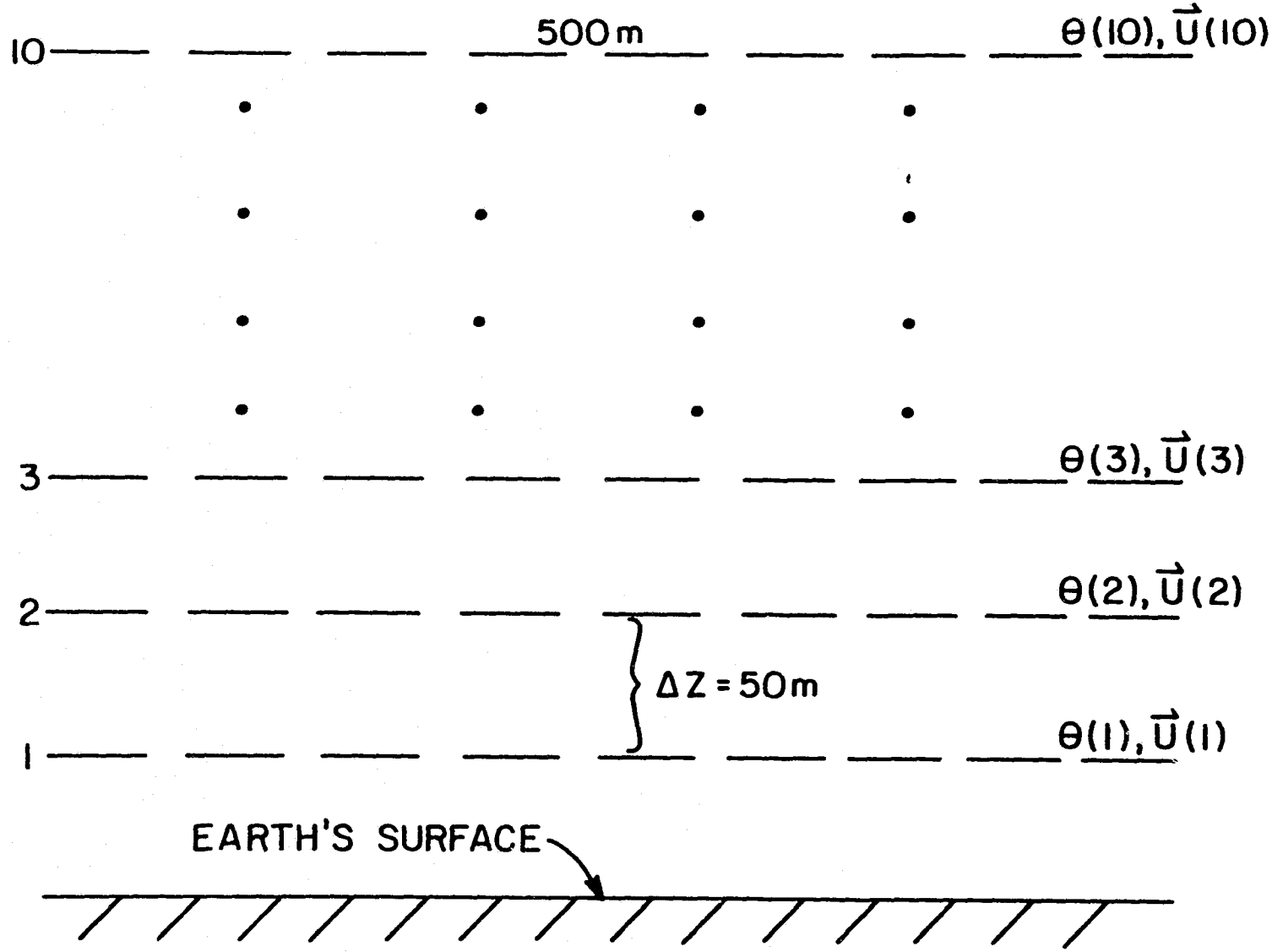

Figure 3. Basic structure of nocturnal component of model.

layer outlined above has been implemented. Forward differencing is used and a time step of 120s has been found adequate to insure computational stability.

Initially the 500 meter layer is assumed to be well-mixed and the vertical distribution of θ is set equal to a constant θ_A at the time of the stability reversal, which is reasonable for late afternoon on a sunny day. The vertical shear of the geostrophic wind is determined from an analysis of local surface fields of temperature and pressure; usually only one or two additional wind observations above the surface layer are available. In order to fit a profile for the actual winds to the observations, free convection scaling is assumed to govern the wind profile prior to the vanishing of the upward heat flux. The assumption of free convection scaling assumes that turbulence in the lower part of the mixed layer is buoyantly driven (Tennekes, 1970), and provides a relationship for the wind shear

$$\frac{\partial U}{\partial z} = bz^{-4/3} \tag{31}$$

which leads to a velocity defect expression

$$U - U_{obs} = bz^{-1/3} \tag{32}$$

where b is determined empirically and z is measured downward from z_{obs} (where z=0 and $U=U_{obs}$). Equation 31 is applied to 00Z wind data for the layer between the top of the surface layer at 50 meters and 200 meters; above 200 meters the wind is assumed initially to be constant with height

to 500 meters. The complete form of the late afternoon wind and temperature profiles is represented in Figure 4. The specified initial wind profile may possess a significant ageostrophic component but the model has been found to adjust smoothly to the transition during the first hour or two of integration beyond the time of reversal in the sign of the heat flux, ultimately achieving a quasi-equilibrium with small accelerations.

The value of the bulk Richardson number defines three stability classifications for which events in the surface layer will be quite dissimilar:

(I)	$B<0$,	UNSTABLE
(II)	$0\leq B\leq .2$,	STABLE
(III)	$B>.2$,	NON-TURBULENT

In cases I and II the surface heat flux is given by equation 23 and will be positive when the surface layer is unstable (a situation which will rarely occur at night), and negative (downward directed) if stable. For case III the surface layer will be decoupled from events above 50 meters because of the strongly stable lapse rate near the ground ($\theta(50m)>\theta_g$); both u_* and H_o will then become zero.

A typical sequence of events near sunset would follow a progression through the three stability classifications outlined above with the surface layer, initially unstable, becoming stable (B increasing). As the ground temperature and wind shear stress decrease rapidly, the stratification will act to decouple the surface layer from the atmosphere above. As the stress decreases and the turbulence near the

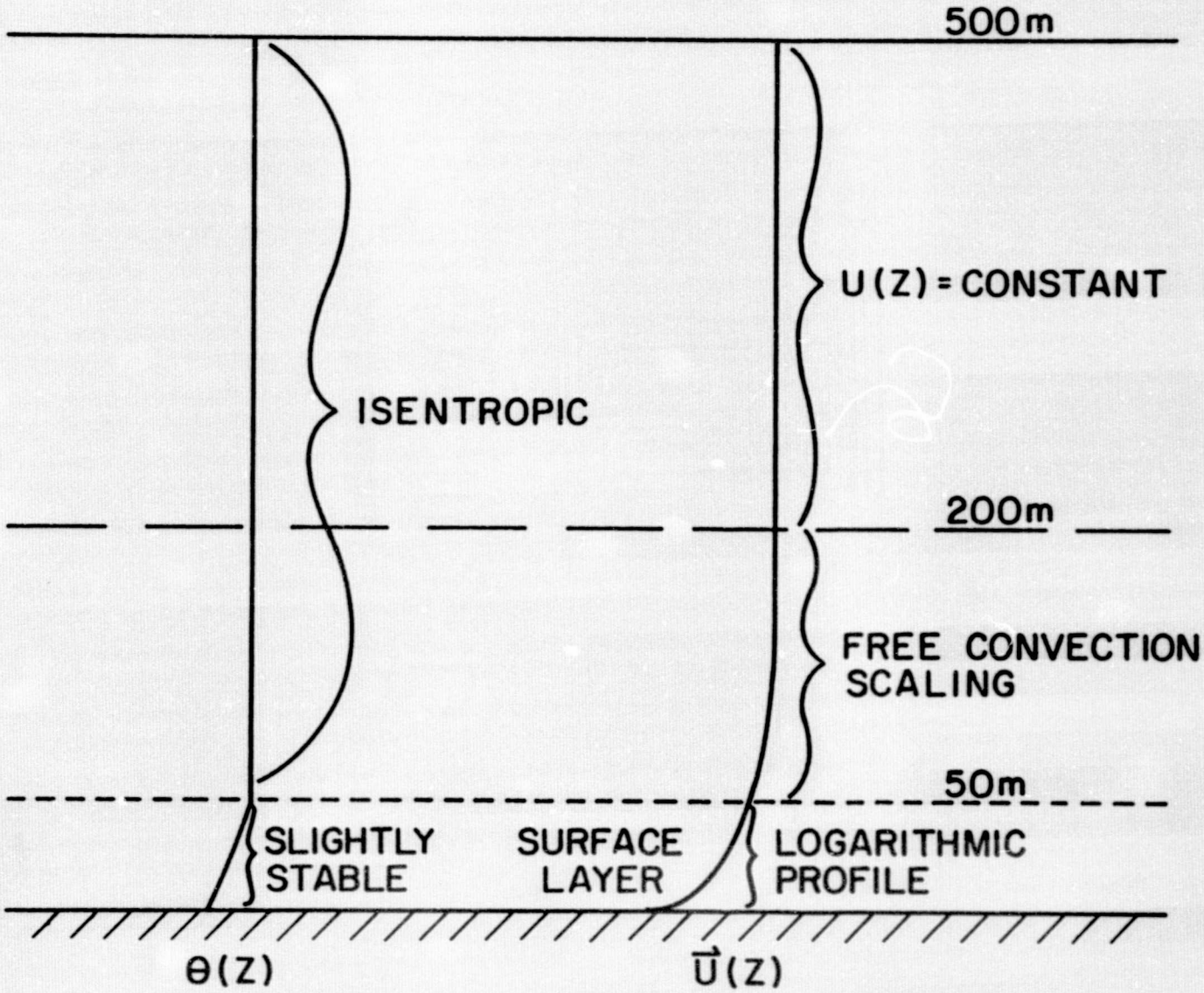

Figure 4. Schematic of initial wind and temperature profiles for the nocturnal component of model.

ground ceases (B>.2), the wind above will accelerate, increasing the vertical shear. If this shear becomes large enough B may fall below 0.2, allowing a turbulent event to occur with a downward directed exchange of heat which will act to elevate the ground temperature for a time. Such turbulence may continue to recur throughout the night. While the model will certainly not have much accuracy in timing these events, numerical tests demonstrate that this formulation successfully predicts which nights are likely to experience turbulent episodes. The governing parameter for these events is the geostrophic wind (assumed constant with time). On nights when the surface geostrophic wind is large turbulent events are more likely.

An important aspect of the nocturnal model is the manner in which the surface temperature is calculated. During the day the surface layer is buoyantly driven and the heat flux will determine the thermal response of the ground and atmosphere to the solar radiation. At night, however, H_o often becomes zero and is passively dependent on the vertical temperature distribution. Because the integral I in equation 8 diverges toward infinity when the heat flux approaches zero, the energy balance at the surface is used directly to solve for the surface temperature. Equating the right hand sides of 1 and 2 and solving for T_o produces the quartic equation

$$AT_o^4 + BT_o + C = 0 \tag{33}$$

where

$$A = \varepsilon_g \sigma \tag{33a}$$

$$B = \lambda/\Delta z \tag{33b}$$

and

$$C = \lambda T_{-1}/\Delta z + H_o + E_o - \varepsilon_A \sigma T_A^4 + S \quad . \tag{33c}$$

At each time step Newton's technique for finding real zeros of a polynomial is iterated until the above expression converges to the correct value for T_o. At night in the non-turbulent surface layer H_o, E_o, and S are zero so that equation 33 expresses a balance between the longwave terrestrial radiation and the ground heat flux. As such, the value of λ_1, the thermal conductivity, is an important determinant in the nighttime behavior of T_o.

2.2 Data Reduction and Analysis

During the past decade several meteorological satellites with the capacity to provide high-resolution thermal mapping of the earth's surface have been placed in orbit. Three of these types, the Geostationary Orbiting Environmental Satellite (GOES), the National Oceanic and Atmospheric Administration (NOAA) satellites, and the NOAA TIROS-N satellites possess sufficient resolution (.5 - 1 km) to allow spatial representation of surface temperature (I.R. derived) and albedo (visible channel) to be made on a scale necessary for resolving details of the urban-rural canopy. Polar orbiting vehicles, however, are capable of measuring the diurnal temperature cycle, and, until recently, were set to scan at hours shortly after sunrise and sunset. Recently, the Heat Capacity and Mapping Mission (HCMM) satellite was

launched by NASA to provide high resolution (.5 km) measurements of the radiometric ground temperature with overhead passes occurring very close to the times of local maximum and minimum temperatures; approximately 2 P.M. and 2 A.M. respectively. Because of its schedule, the HCMM satellite will be used to provide data for the present research; in the future TIROS-N data may be used because of its high quality and more frequent availability of day-night image pairs at these times.

The procedure of data reduction to arrive at maps of surface temperature follows an approach described by Augustine (1978). A sequence of computer programs is used to extract the raw data from tape, grid the location of the working area, apply a calibration to the digital counts and ultimately to produce maps of blackbody surface temperature. A schematic representation of this procedure is shown in Figure 5. The first step is to transfer onto a standard labeled tape a smaller more manageable area from the raw data tape obtained from NASA. This subset will have digital count information (DN values) in a 512 x 512 matrix where, for the polar orbiting HCMM satellite, the pixel and scan line densities are approximately equal at the sub-satellite point. The subset area contains the region to be analyzed and is located geographically using the appropriate image for that same data set. From the larger matrix a 130 x 130 working area of about 4225 km^2 is extracted which will center on the particular region to be analyzed. A histogram of the count value density is also extracted and this provides information on the temperature distribution in the working area. The histogram allows a slicing of the data according to a user-defined alphanumeric code whereby the DN values are transferred into characters and written to output. The character

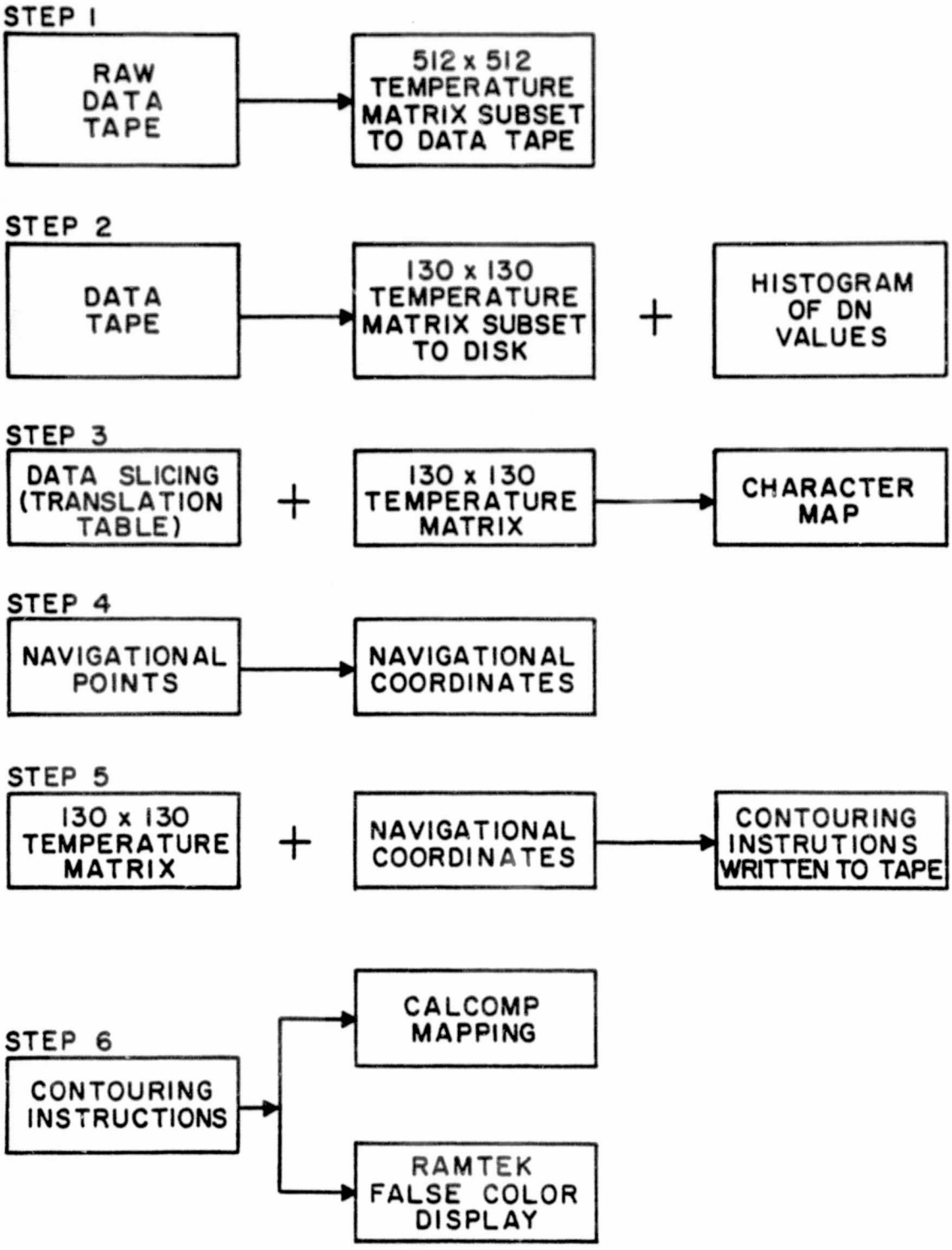

Figure 5. Schematic diagram of the satellite data processing procedure.

map of the working area allows the identification of geographic features (parks, coastline, rivers) to which latitude and longitude values are assigned. Using these navigational points another utility program is run which uses regression analysis to produce coordinate labeling of the working area's boundaries. The matrix of DN values is subsequently converted to surface temperatures which are then drawn by computer on a gridded background. Before the analysis can be completed digital count values are equated to temperature using the calibration equation for the HCMM data which has a temperature range of 260° - 340°K representing the count values of 0 - 255. A water vapor correction suggested by Cogan and Willand (1974) is also applied prior to the graphing procedure.

This final analysis can now be displayed in various ways. One procedure involves mapping the working area in a geographical framework suitable for identifying urban features or for investigating surface temperature as a function of land use and ground cover type. In this approach a CALCOMP plotter is used to produce an objective contouring of temperatures over the working area with the navigational references labelled on the border. An example of such a mapping for Los Angeles is shown in Figure 6 in which the coastal and urban temperature features are clearly evident. Another type of final product used as an aide in locating surface features for gridding is a false-color-enhanced image created by a RAMTEK color display monitor where the color scale may be manipulated by the user to accentuate features such as urban-rural temperature differences, mountains, clouds, etc. A black-and-white copy representing the same Los Angeles study as above is shown in Figure 7 with lighter areas corresponding to higher temperatures.

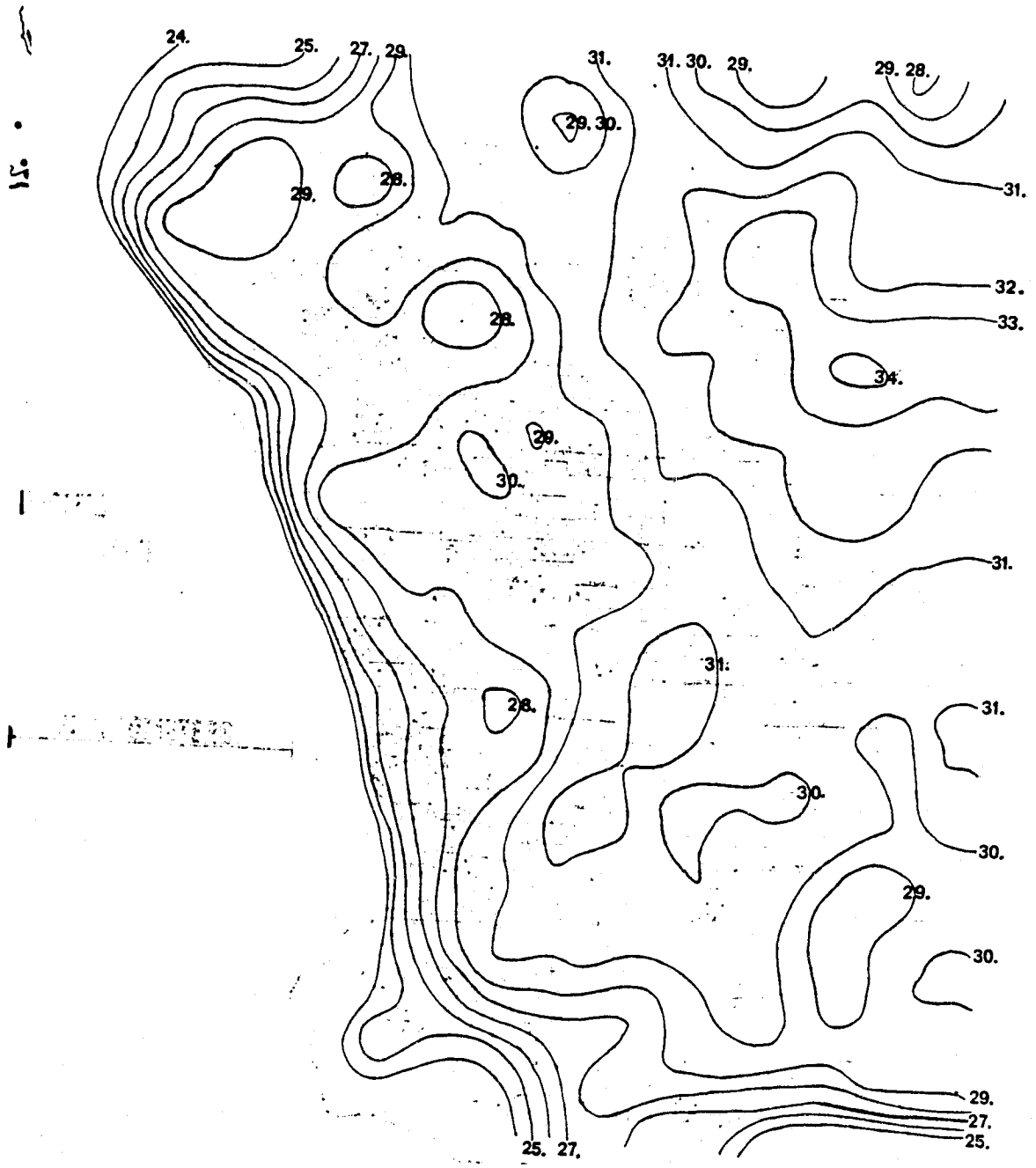

Figure 6. Example of daytime surface temperature mapping across Los Angeles for May 31, 1978.

Figure 7. Example of RAMTEK graphics for daytime surface temperatures across Los Angeles, May 31, 1978.

Although these contoured and false-color-enhanced canvasses of urban scale ground temperature variations are informative on their own, the present research goes well beyond a simple temperature analysis. As stated in section 1.3, the final goal is to produce maps of moisture availability, thermal inertia, and daytime heat and moisture flux at the surface. Accordingly, it is necessary to consider both day and night temperatures, since further manipulation of the reduced temperature data is necessary to arrive at these fields. Thus, the surface temperatures were stored as a function of their position within the original working area on a grid in which the coordinates are not longitude and latitude but an arbitrary set of reference coordinates, one for each region of interest. Subsequent manipulation of the day-night temperature images which have been rectified to this new grid system will be discussed in the next section.

2.3 Coordination of Model Output and Satellite Data

As mentioned in section 1.3, the approach in deriving (or, more precisely, inferring) the maps of M, P, H_o and E_o will require combining the observed temperatures with output from the boundary layer model. In principle, if the functional forms of the expressions governing the surface fluxes were simple, the model equations could be analytically solved for these fluxes. Because of the complexity of the surface layer model and the solar geometry, a facile solution is impossible and it is necessary to determine the relationship between the model values of M, P and the surface fluxes and the observed day-night temperature fields by a series of regression equations which represent these relationships determined from the model output. A

pair of day and night temperature fields, each representing a 130 x 130 working area, constitutes the initial data set for obtaining the terrain parameters and surface fluxes. Rather than embracing the awkward notation of degrees longitude and latitude, it has been found convenient to define a fixed topographical coordinate system (TOPO-coordinates) and represent the temperature and all other fields within a common reference frame whose coordinates are assigned integer values. The final analyses are ultimately transferred back into geographical coordinates for display and interpretation. A schematic representation of the entire analysis procedure is shown in Figure 8.

Because the day and night pixels are initially not exactly coincident, a utility program (REGGIE) was used to transform the day and night temperatures from their 130 x 130 working areas onto a smaller TOPO area which is a subset of the region common to both the daytime and nighttime working areas. This subset TOPO grid is represented in Figure 9. Note that the image areas are oriented 20° - 30° from each other. The extraction of the TOPO subset area reduces the effective working area to a region which was arbitrarily arranged to contain about 100 x 100 TOPO subgrid intersections over an area of approximately 2000 km^2.

Such a reduced region will nevertheless be large enough to include even the largest urban centers although care must be exercised in the initial extraction of the two working areas such that the common TOPO subset remains within both of the initial 130 x 130 working areas while the size of the TOPO subset is still maximized. The final output of REGGIE is two files, one containing the subgrid TOPO coordinates, the other the temperature pair of each point within the TOPO subgrid.

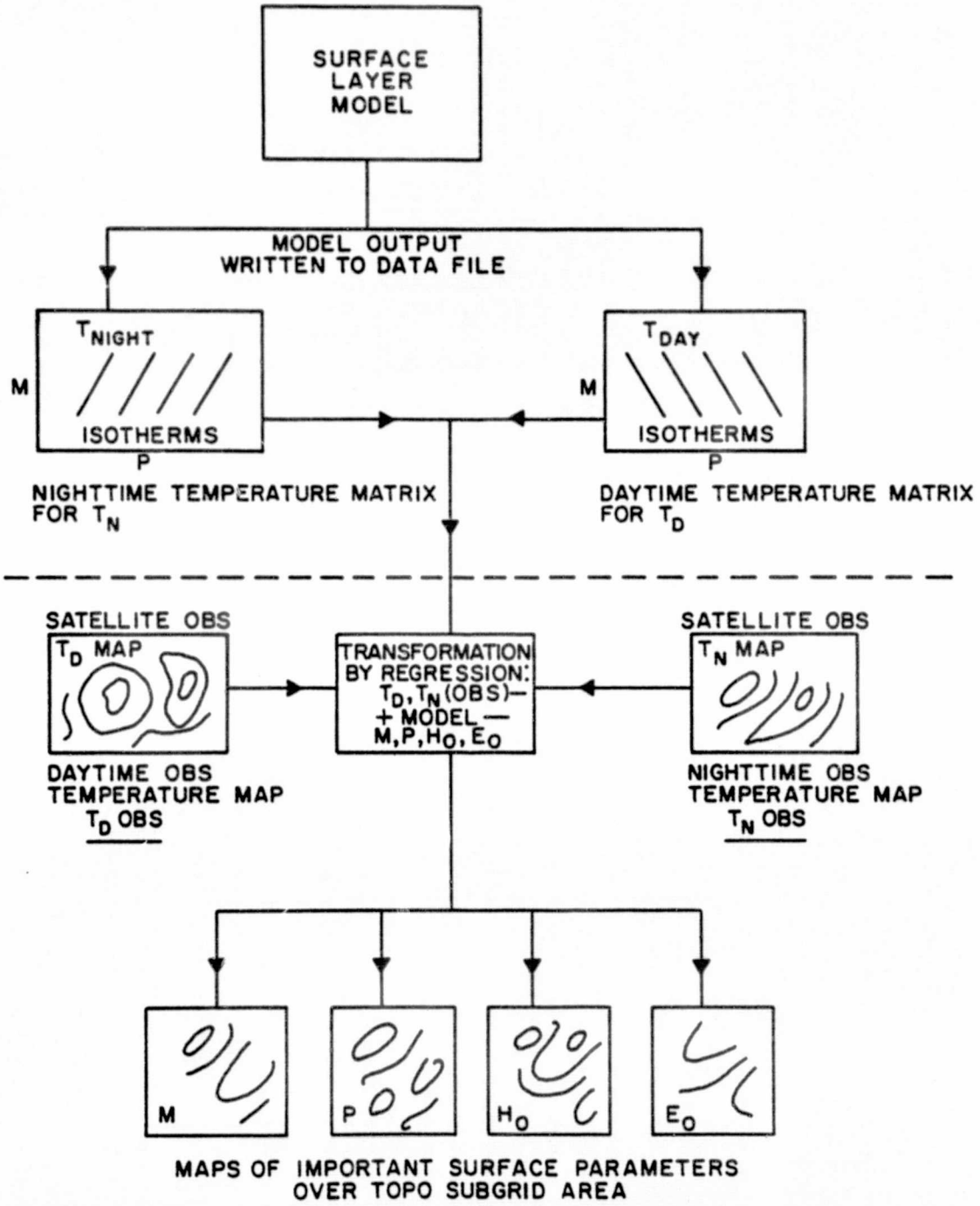

Figure 8. Flow diagram for inferring surface parameters.

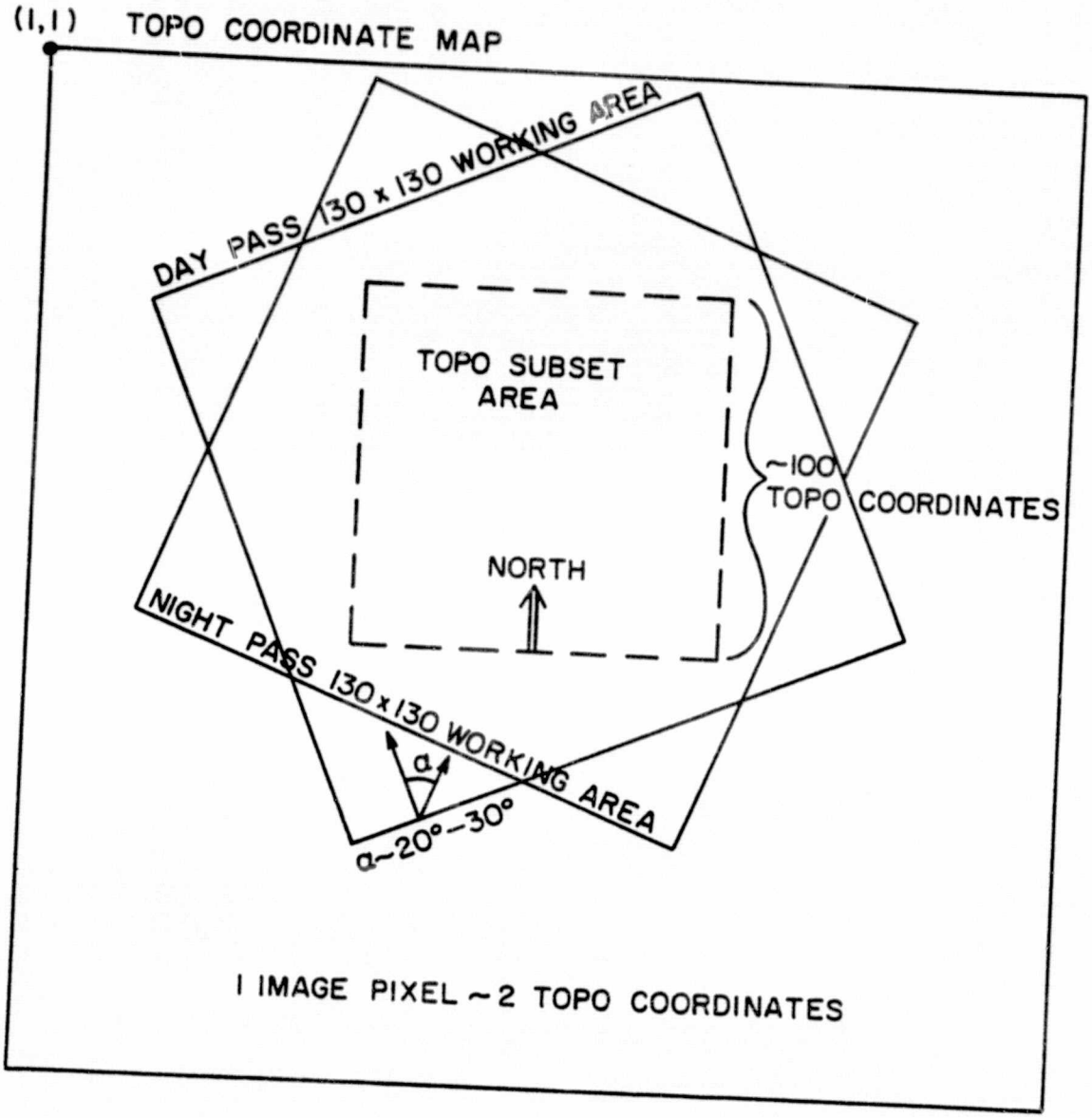

Figure 9. Schematic representation of TOPO subset area.

The other component necessary before the final analysis can be performed is output from the model which will produce temperature as a function of M and P. For each case study the weather situation was studied and the model carefully initialized using a morning surface weather map and the 00Z upper air data as stated in section 2.1. An accurate initialization is crucial in assuring that the model will yield results which are compatible with the observed temperature fields.

Typically, the model is initialized at a time near sunrise and allowed to proceed for about 22 hours. The fundamental parameters, M and P, are set equal to .05 and .005 in the first cycle but upon completion of each 22-hour period, the model is re-initialized with an incremented value of M(.3, .55,...) and P(.03,.055,...) while all other conditions remain the same. Each cycle yields a day and night temperature appropriate to the times of satellite overflight and corresponds to a unique M, P pair. A graphical representation of the solutions for the relationship between M, P and surface temperature is illustrated in Figure 10. In this diagram the full range of physically realistic values of thermal inertia (.005 - .1) and moisture availability (.05 - 1) corresponds to a field which encompasses a unique solution for a given pair of observed temperatures, which are those intersections of the day and night temperature curves. For HCMM or TIROS-N, the times of overflight occur near those of the diurnal maximum and minimum temperature or heat flux, approximately 2:00 A.M. and 2:00 P.M. For those times, the model output (M, P, H_o, E_o, T_g, etc.) was written to a data file for further manipulation. It was found that an essentially complete solution for M and P could be determined with reasonable accuracy after the model had been cycled through 16 times. Thus 32

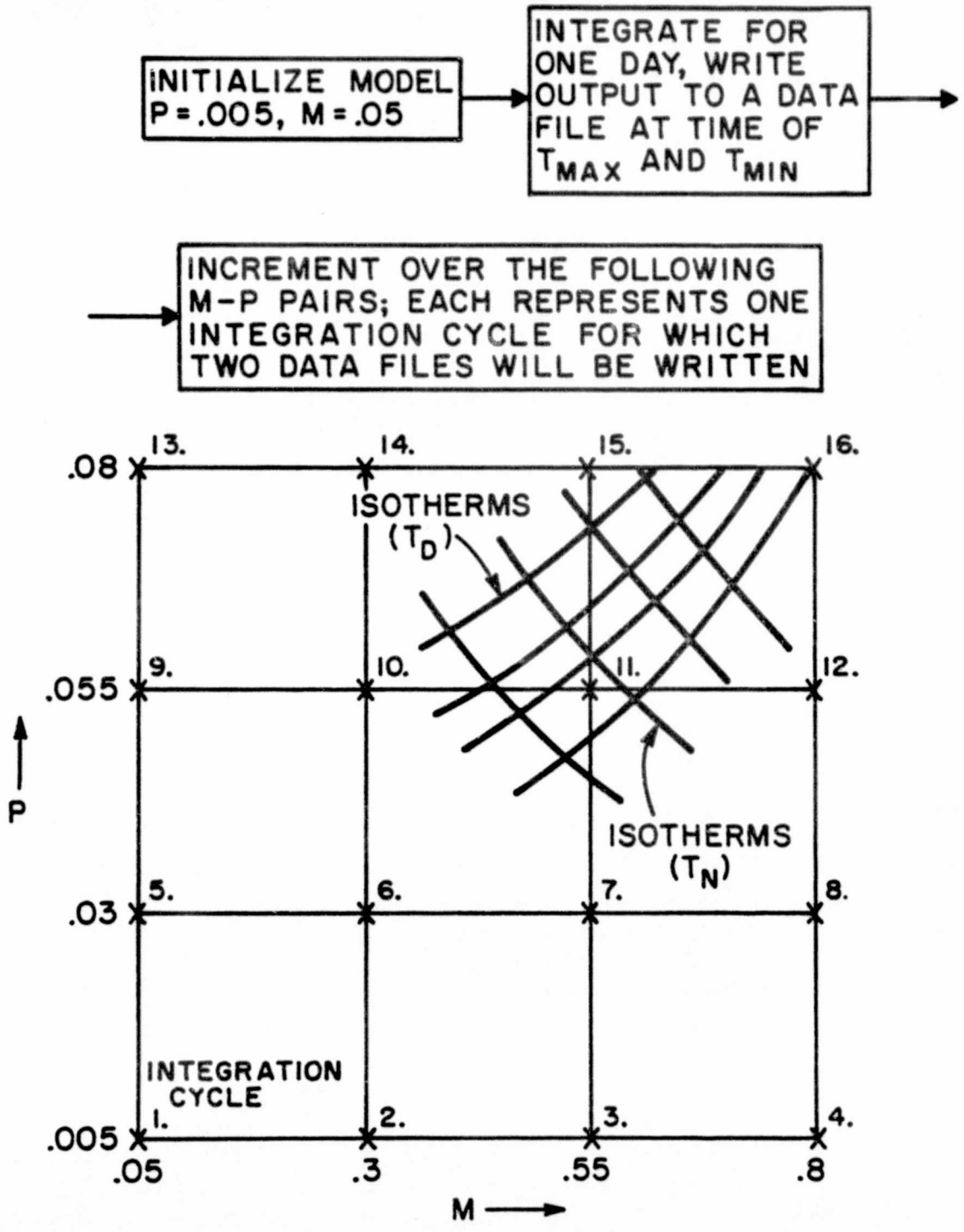

Figure 10. Schematic illustration of incrementation process and day-night temperature arrays.

records of output information representing 16 unique M, P pairs were used to construct a set of relationships between the simulated temperatures and the respective values of M and P.

The next step in the analysis procedure was to derive quadratic equations for M, P, H_o and E_o as a function of the day-night temperature pairs (T_d, T_N). These equations were obtained from a regression analysis (MINITAB II) of the model output and are expressed generally as

$$M = C_1 + C_2T_d + C_3T_d^2 + C_4T_N + C_5T_N^2 \tag{34}$$

$$P = C_6 + C_7T_d + C_8T_d^2 + C_9T_N + C_{10}T_N^2 \tag{35}$$

$$H_o = C_{11} + C_{12}T_d + C_{13}T_d^2 + C_{14}T_N + C_{15}T_N^2 \tag{36}$$

$$E_o = C_{16} + C_{17}T_d + C_{18}T_d^2 + C_{19}T_N + C_{20}T_N^2 \tag{37}$$

where the coefficients are written to a data file. In this way, thermal inertia, moisture availability, sensible heat flux, and evaporative heat flux are determined from the model results and subsequently combined with the observed satellite temperatures within the TOPO grid to produce the final products which are fields of heat and moisture flux, and the parameters M and P. Accordingly, the last step in the analysis procedure involves a convolution of the regression coefficients with the temperature data in the TOPO grid to create maps of M, P, H_o, and E_o over the domain contained within the TOPO subgrid. To accomplish this task, a final system program, PROVALS, is implemented which uses the satellite day-night temperature pairs from REGGIE

and the coefficient file to calculate values of M, P, H_o, and E_o within the 100 x 100 TOPO subgrid. The TOPO coordinates are then transferred back into latitude and longitude and the matrices of M, P, H_o, and E_o values are written to another data file which was used to graph the analysis. The procedure previously described for mapping temperatures is also used for mapping these other fields. The results are presented in this thesis as isopleths on conventional map backgrounds; however a capability exists for displaying the fields using RAMTEK false-color graphics.

3.0 RESULTS

3.1 Background

The Heat Capacity Mapping Mission (HCMM) satellite day-night data tapes containing surface blackbody temperature measurements were obtained from the National Aeronautics and Space Administration (NASA). The orbital characteristics of the HCMM satellite are contained in Table 1. These data were used in conjunction with the surface layer model to infer the surface energy budget and terrain parameters using the method described in the previous chapter. The data pertain to two urban areas, the Los Angeles Basin and the St. Louis area including the surrounding suburbs. Both locations are highly urbanized and exhibit important anomalies in temperature and other meteorological parameters in a manner which is peculiar to the urban microclimate. The working areas chosen for analysis also contain sizeable areas with little or no urban sprawl and thus have not yet become substantially modified from their natural state; these areas will provide an interesting contrast with the urban centers where values of temperature, moisture availability, thermal inertia, and heat flux differ greatly from those over the surrounding countryside.

The extracted working areas cover approximately 2000 km^2 and center on the commercial centers of Los Angeles and St. Louis, the dates being May 30-31 and June 9-10, 1978, respectively. Figures 11 and 12 display base maps for the appropriate city and contain a letter key for identifying specific locations which are to be referenced in subsequent discussion. As described in the previous chapter, the boundaries of the final analysis are contained within an area common

Figure 11. A population density map of the Los Angeles area with a letter key marking areas of interest references in the text.

B Bellflower

BH Baldwin Hills

C Downtown Business District

CC Compton

I Maywood Industrial Site

IN Inglewood Country Club

PV Palos Verdes Penninsula

RH Rancho/Hillcrest Park

SM Santa Monica Mountains

T Torrance

U USC Campus

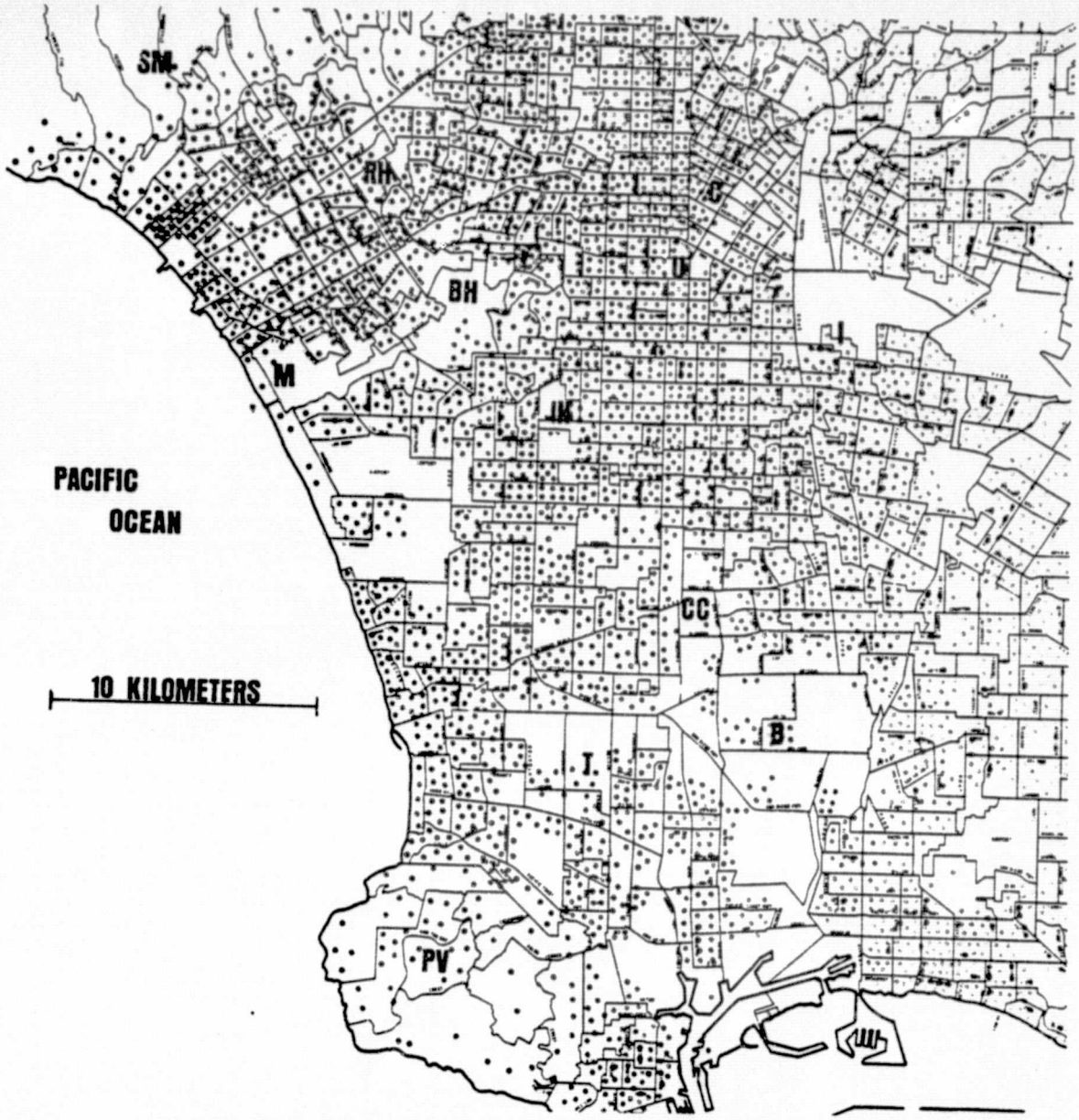

Figure 12. A road map of St. Louis and vicinity with a letter key marking areas of interest referenced in the text.

C Cropland-Pasture Sites

D Downtown St. Louis

E East St. Louis

F Deciduous Forest

FP Forest Park

G Granite City

H Horseshoe Lake

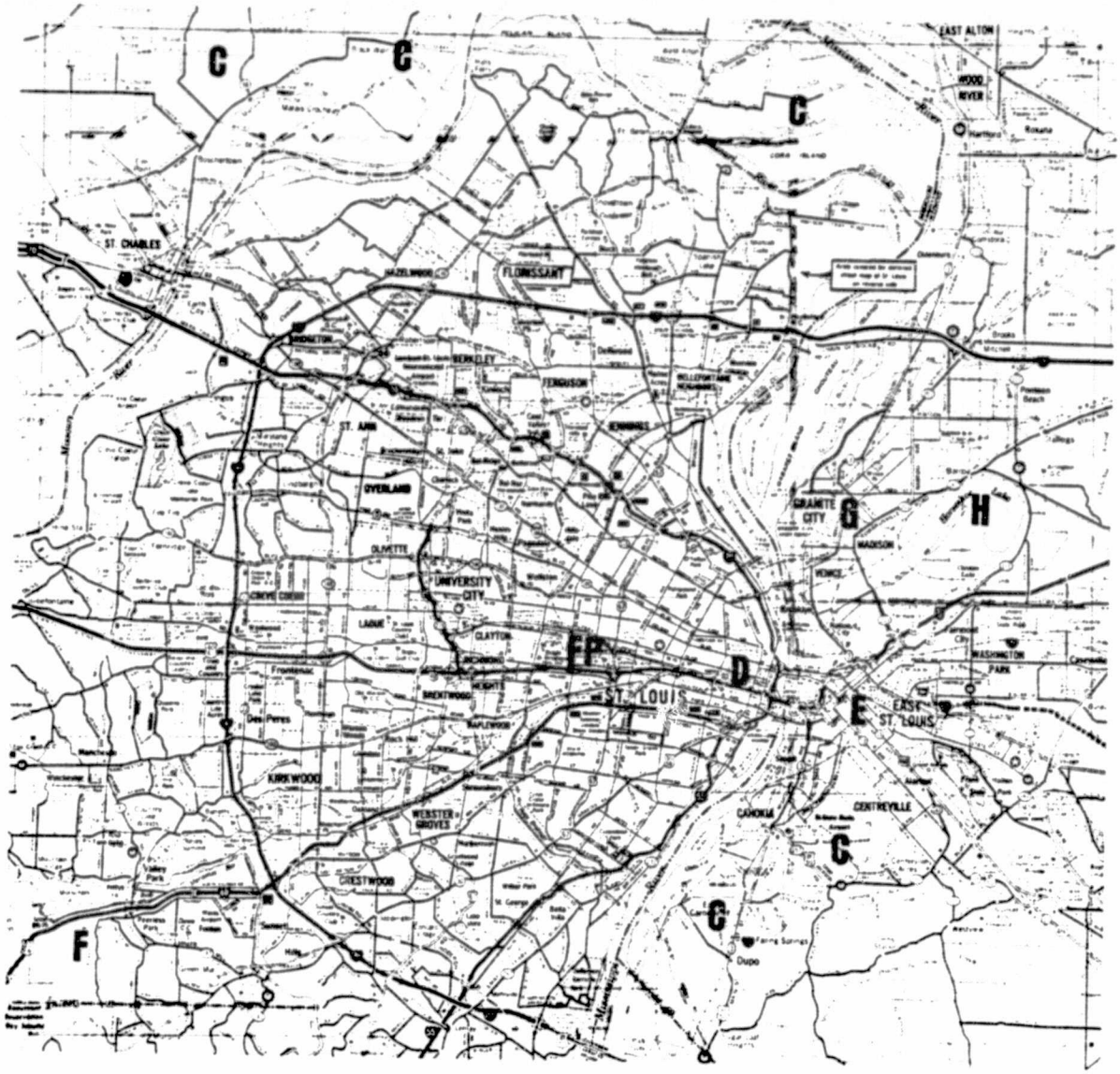

TABLE 1. HCMM Satellite Orbital and Radiometer Characteristics

Orbital Altitude	620 km
Angular Resolution	0.83 milleradians
Resolution	0.6 x 0.6 km at nadir
Scan Angle	60°
Scan Rate	14 revolutions/second
Sampling Interval	9.2 microseconds
Swath Width	716 km
Thermal Channel	10.5 to 12.5 microns
Usable Range	260° to 340° K

to both the day and night working areas. Ideally, the day and night images will pertain to data 12 hours apart, at times when the daytime and nighttime temperatures are close to those of the maximum and minimum values in the same diurnal cycle. Unfortunately, 12-hour coverage was unavailable for this study and both cases analyzed utilize day and night image data which are separated by 36 hours, the daytime data corresponding to measurements made a day and one half after the nighttime satellite pass. This situation will, of course, necessitate some additional assumptions concerning the stationarity of the diurnal temperature wave.

For each case study the model was carefully initialized using hourly surface observations and vertical soundings for 00Z and 12Z. A full summary of the specific values of initialized quantities is

presented in Table 2. In the case of the Los Angeles data it was found that an acceptable assumption was that the surface temperature changes little from one afternoon to the next (or from one morning to the next). Therefore the model was still cycled through a 22-hour period but the 2 P.M. (daytime) observations were treated as though they were 12 hours apart rather than 36 hours, a reasonable approximation in view of the usually small day to day variability in weather over the Los Angeles Basin during the late spring and summer. Therefore, after the model was cycled for pairs of M and P it was reinitialized for each subsequent cycle and the output information stored for times corresponding to the day and night satellite observations.

For the St. Louis case a large high pressure area of unseasonably cool air was moving eastward across the center of the country during the 48-hour period prior to June 10. This weather pattern resulted in much colder temperatures being recorded the morning of the 9th than the morning of the 10th, when southerly flow commenced and temperatures moderated. Due to an apparent warming trend, the model was initialized at 6 A.M. for conditions appropriate to the 9th and cycled over a 36-hour period for each M and P pair to yield first a simulated nighttime temperature followed by a succeeding daytime temperature. Although the model was reinitialized at 6 A.M., the change of air mass was simulated by including in the ground a realistic initial vertical temperature distribution which provides a variable surface initialization for each M and P pair. It is felt that in the absence of 12-hour data pairs the variable initialization should represent a more accurate set of conditions than would be the case for an initialization which does not vary between each cycle.

TABLE 2. Model Input Parameters for Case Studies

CASE	T_g	T_A	Z_o	$\bar{U}_A$	q_A	W	A_o	ε_g
Los Angeles	289.0	290.0	30.0	552.0	.009	1.1	.19	.95
St. Louis	282.0	286.0	30.0	600.0	.007	.74	.17	1.0
Units	°K	°K	cm	cm/sec	ND*	cm	ND*	ND*

Since the model will be used to infer a field of values it is evident that the variable initialization and 36-hour cycling interval provides some initial spatial hetergeneity which can compensate for the observed warming trend and also simulate inherent variations in this warming due to terrain irregularities.

It should be noted that for both case studies the nighttime (2 A.M.) satellite overpass occurred prior to the daytime (2 P.M.) overpass. For the St. Louis case, the nighttime model temperatures correspond to a time before that of the daytime output. However, for the Los Angeles case the simulated daytime temperatures actually occur before the night (i.e., in reverse order of the actual observations), although the order in which the temperature pairs are generated in the model is not thought to be a significant source of error because of the stationarity of the temperature cycle and slowly changing nature of the Los Angeles weather. In principle, it would be possible to represent the observed 36-hour day and night temperature pairs in the correct sequence within the model by operating over a 60-hour cycle starting 24 hours prior to the nighttime orbit and continuing through the afternoon of the following day at the time of the daytime measurement which occurs on the afternoon 36 hours after the nighttime orbit. Such an extensive cycle would, however, add significant cost to the procedure (since it was found necessary to perform 16 cycles) without contributing very much additional realism.

3.2 Los Angeles May 30 and 31, 1978

The weather during the 36-hour period of May 30-31 was rather typical for late spring in Los Angeles. Skies were clear as the marine layer stratus remained offshore and the sea breeze became established during the afternoon in response to the land-sea temperature gradient. Atmospheric moisture was quite small resulting in a small correction to the derived blackbody temperatures. Precipitation had not occurred over Southern California for several days prior to this period, thus the ground can be expected to be relatively dry.

3.2.1 May 31 Daytime Temperatures, T_D

The daytime thermal map in Figure 13 displays a large area centered on the cities of Maywood and Commerce where the ground temperatures are in excess of 32°C, warmer than at any other location within the Basin. Highest values, in excess of 34°C, are found over the Maywood industrial site (I) where commercial centers, railroads, and heavy industry conglomerate to form a sizeable region in which there is almost no vegetation. The 32°C isotherm extends to the northwest of the industrial area to include the business district of downtown Los Angeles (C), an area several miles square composed of high-rise office buildings, parking lots, and a dense intersecting network of streets. Other local temperature maxima are all related to business or industrial centers such as Compton (CC), the oil refinery sites near Torrance (T), and the commercial district in Bellflower (B).

The most obvious minimum occurs just east of the strong gradient along the coast where the relatively cool ocean (15°C) bounds the

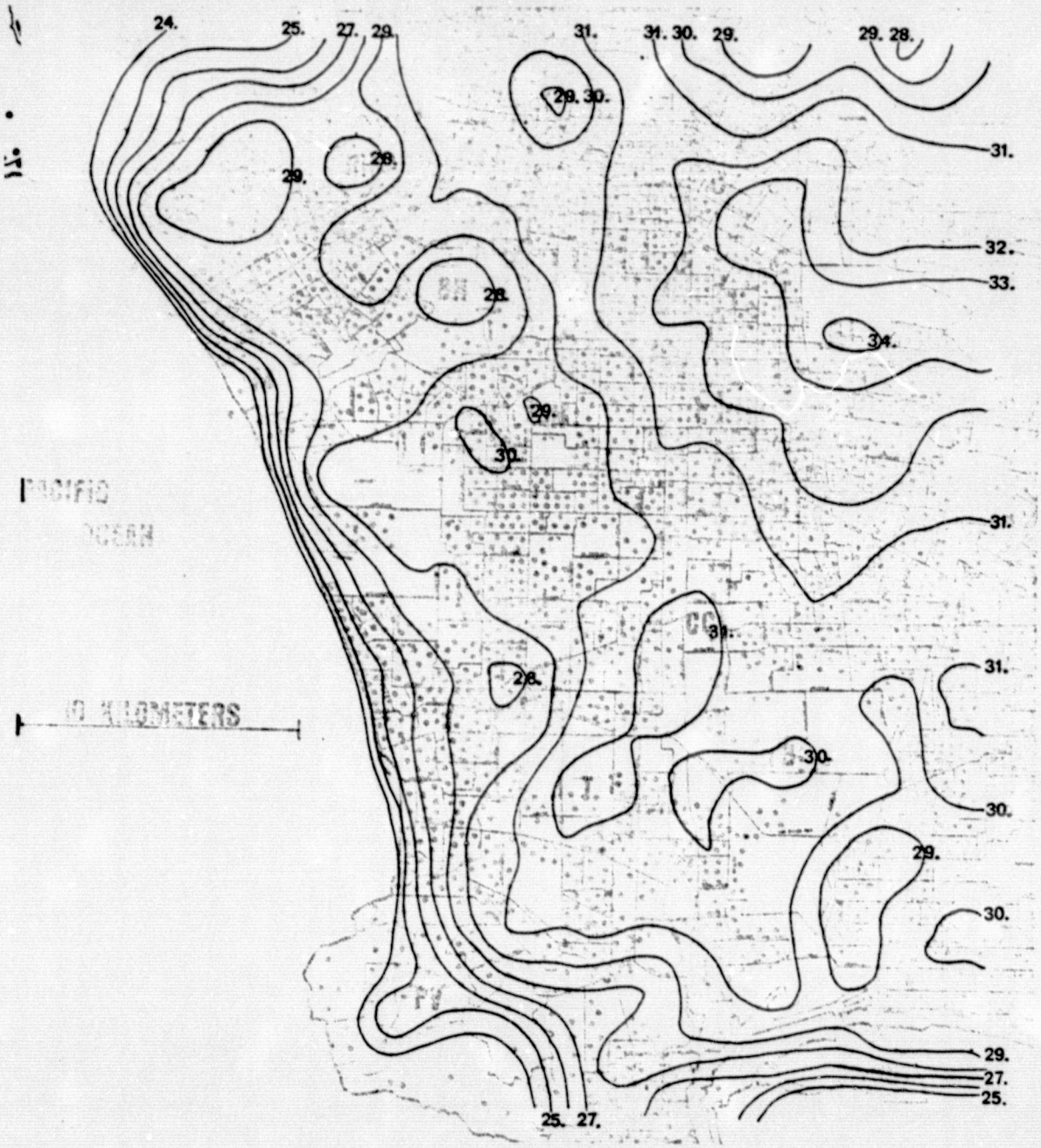

Figure 13. Los Angeles, May 31, 1978 daytime surface temperature analysis.

beaches and beach cities. Other prominent minima occur over the Santa Monica Mountains (SM), which border the Basin to the northwest, the hills immediately north of downtown, and the Palos Verdes Penninsula (PN). The notably lower temperatures (less than 22°C), evident at SM and PV, are likely due to the higher elevation as well as to the higher evaporation potential of these vegetated regions. On the urban plain itself the only other apparent minima center on large grassy areas which include Rancho-Hillcrest Park, Inglewood Country Club, and the Baldwin Hills (RH, I, B). The temperature range over the lower density suburban residential areas which comprise a majority of the Los Angeles Basin exhibits a small temperature variability, between 29° and 31°C.

3.2.2 May 30th Nighttime Temperatures, T_N

The nighttime pattern shown in Figure 14 is certainly less well-defined than the daytime pattern with the range of temperatures between 10° and 13°C over the Basin. In general, temperatures 5 to 10 miles inland are warmer than those near the coast but this is more likely a direct reflection of an urban rather than a marine influence since the wind at night is a weak easterly drainage flow from land to sea. The warmest temperatures exceed 13°C and are centered on a high population density business and residential area near the University of Southern California (USC) campus (U). Since surface features here probably differ little from other districts surrounding the downtown area there is no obvious physical reason for this anomaly; however, an explanation will be offered later. Generally, regions which exhibit a warm daytime anomaly are also the warmest at night although in places this correspondence is weak.

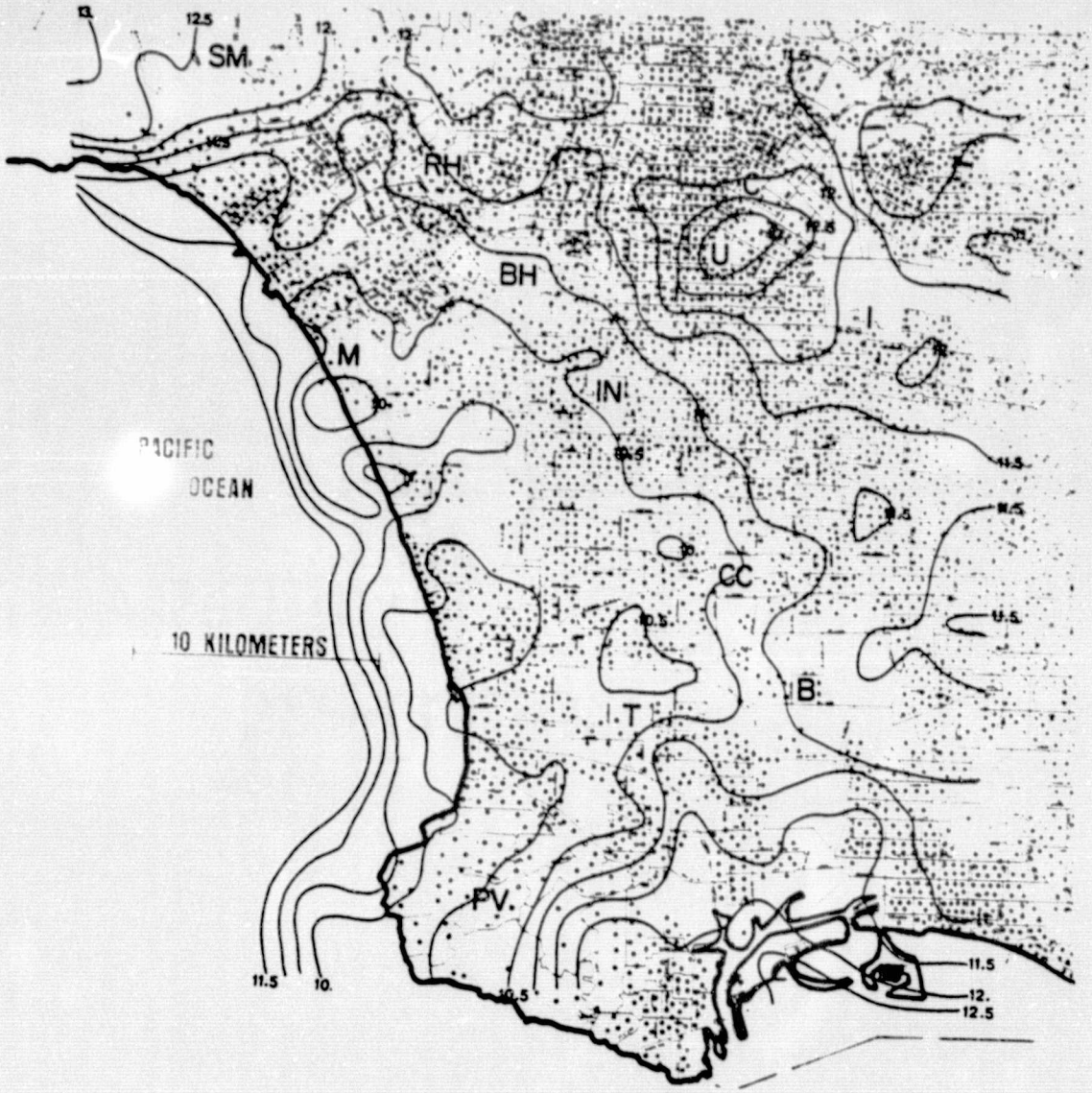

Figure 14. Los Angeles, May 31, 1978 nighttime surface temperature analysis.

It is evident that at night the coastline is poorly defined by the isotherms because the land temperatures do not differ significantly from the ocean. The only distinct feature near the coast is a weak gradient offshore which separates very shallow water along the coast from deeper and warmer water further offshore. Presumably this gradient reflects upwelling along the immediate coastline. Temperature signatures across the remainder of the Basin exhibit rather weak gradients and no other important maxima or minima are present.

3.2.3 May 30-31 Moisture Availability, M

The pattern of moisture availability, M, shown in Figure 15 reveals a striking similarity with the daytime temperature map, maxima of M being highly correlated with temperature minima and vice versa. This inverse relationship is to be expected since a large evaporation potential results in a relatively small portion of the net radiation partitioned as sensible heat flux, a situation which translates into low surface temperatures. Conversely, dry ground suppresses evaporation and allows a greater surface heating. Values of M show a wide range across the domain, from .25 to .75. A large area below .25 centers on the Maywood industrial site (I) extending westward and northward to include most of the downtown business district (C). The surface fabric within this region is a heterogeneous mix of urban materials with vegetation or open fields almost non-existent over areas larger than one acre. The .35 contour encloses approximately one-fourth of the inland working area reflecting the extensive alteration of the surface due to urbanization. Other local minima with M below .35 surround the Compton business district (CC), extending southwest to include the oil refineries near Torrance and Wilmington (T).

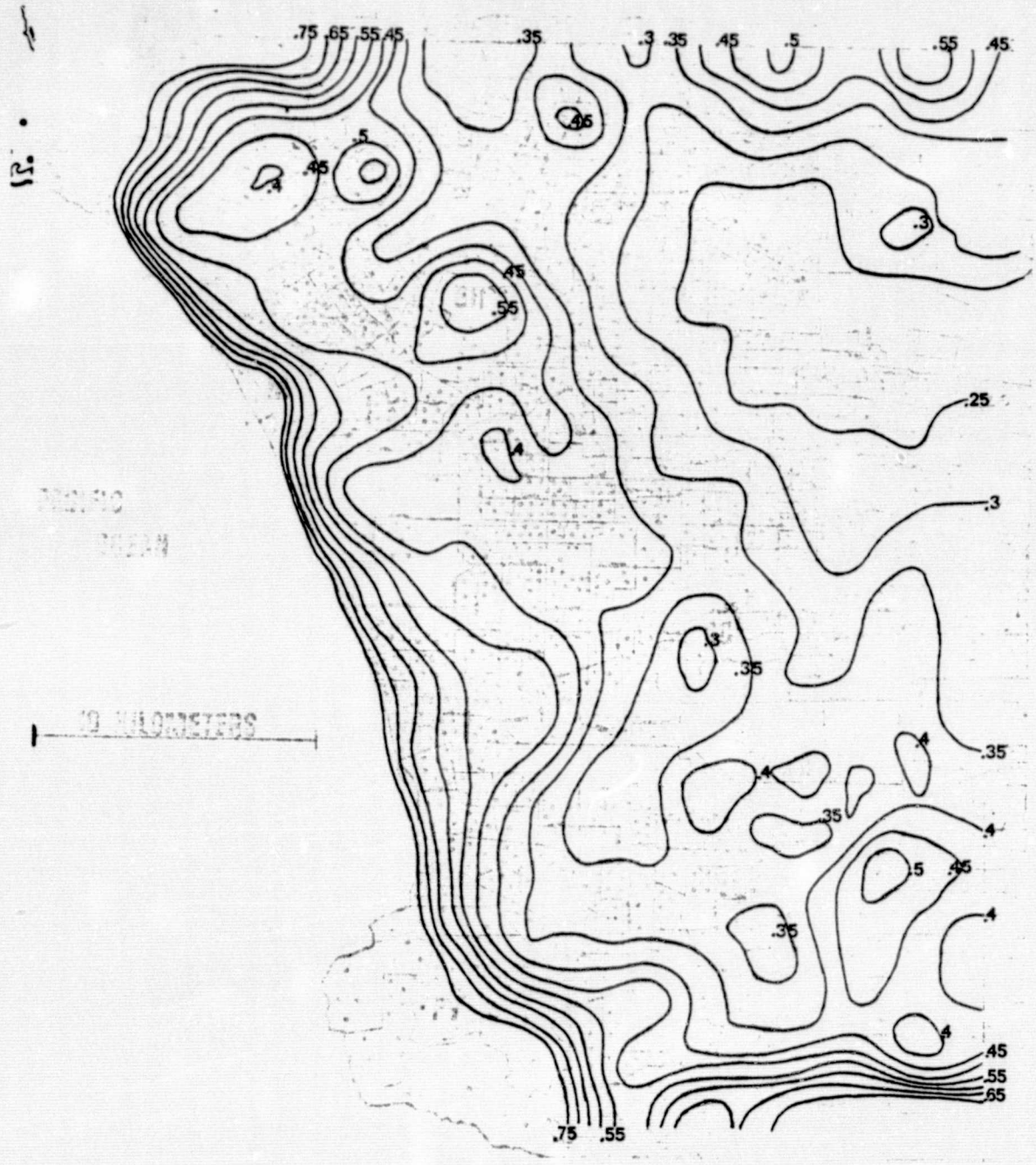

Figure 15. Los Angeles moisture availability analysis.

Local maxima of M are all sparsely populated hilly areas or large parks scattered over the Los Angeles environs. The most prominent maxima include Rancho-Hillcrest Park (RH), the Baldwin Hills (B), and the area of low population density centered on Signal Hill (S) near Long Beach. The Santa Monica Mountains (SM) and Palos Verdes Penninsula (PV) are large areas where the moisture availability was greater than .5. The trend for M to be higher in these areas is reasonable in view of the fact that both sites have small population densities and significant vegetation. It should be pointed out that elevation effects are not included in the model and some error is to be expected in these regions; however, it is felt that an accurate representation of the spatial variability is fundamentally more important than the exact values of the parameters at any point. As in the daytime temperature pattern (Figure 13) the coastline again corresponds to a strong gradient in M although smoothing the data tends to widen the strong gradient which would likely be discontinuous along the coast. In general, M values of about .7 for completely vegetated areas, .4 for suburban sites, and .3 or less for the industrial and commercial districts appear to be representative for the Los Angeles area in this case.

3.2.4 May 30-31 Thermal Inertia, P

The map of thermal inertia presents a distribution unexpectedly lacking in focus. This quantity is thought to vary significantly across an urban domain and is presumed to be largely responsible for determining the nighttime urban temperature pattern. The values shown in Figure 16, however, reflect a rather small variability with

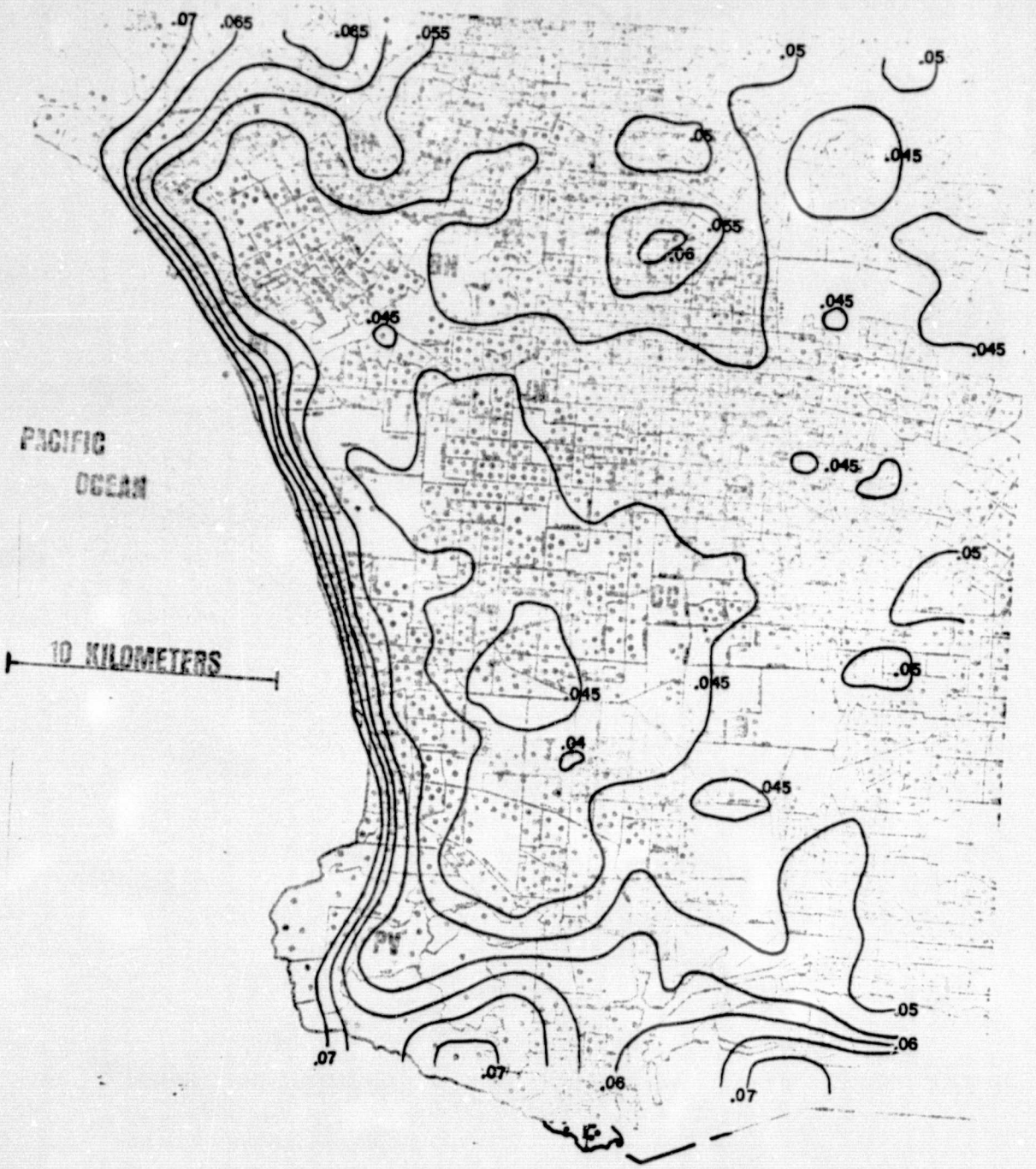

Figure 16. Los Angeles thermal inertia analysis.

P generally restricted between .04 and .05. The one obvious exception is a maximum centered near the USC campus (U) where P exceeds .06. This is the same location which exhibited the maximum nighttime temperature anomaly and is quite close to the Los Angeles civic center (C). The pattern of P over the Santa Monica Mountains (SM) and Palos Verdes (PV) again appears to be somewhat distorted due to the elevation; however, a strong gradient coincides with the coastline although the smoothing of data undoubtedly broadens the gradient near the coast.

No other pronounced maxima or minima of thermal inertia appear in the analysis and the distribution across the entire Los Angeles Basin is remarkably uniform except for the one strong maximum.

3.2.5 May 31 Surface Heat Flux, H_o

Perhaps the most interesting analysis to be discussed is that of the surface heat flux which is displayed in Figure 17. This figure, showing the inferred surface heat flux at 2:30 P.M., offers a unique picture of the variation of H_o across a heterogeneous urban domain. As anticipated, the maximum values appear centered in the same area where the largest daytime temperature anomaly is found, the 202 w/m^2 contour enclosing almost exactly the same region as the 33°C temperature contour in Figure 3.3. A strong maxima is located at the Compton commercial district (CC) extending southwest to the oil refinery site near Torrance (T).

Regions of relative minima, where the heat flux is less than half that in the downtown area, are centered over the Baldwin Hills (B) and at Marina Del Rey (MD), the latter being a man-made marina which

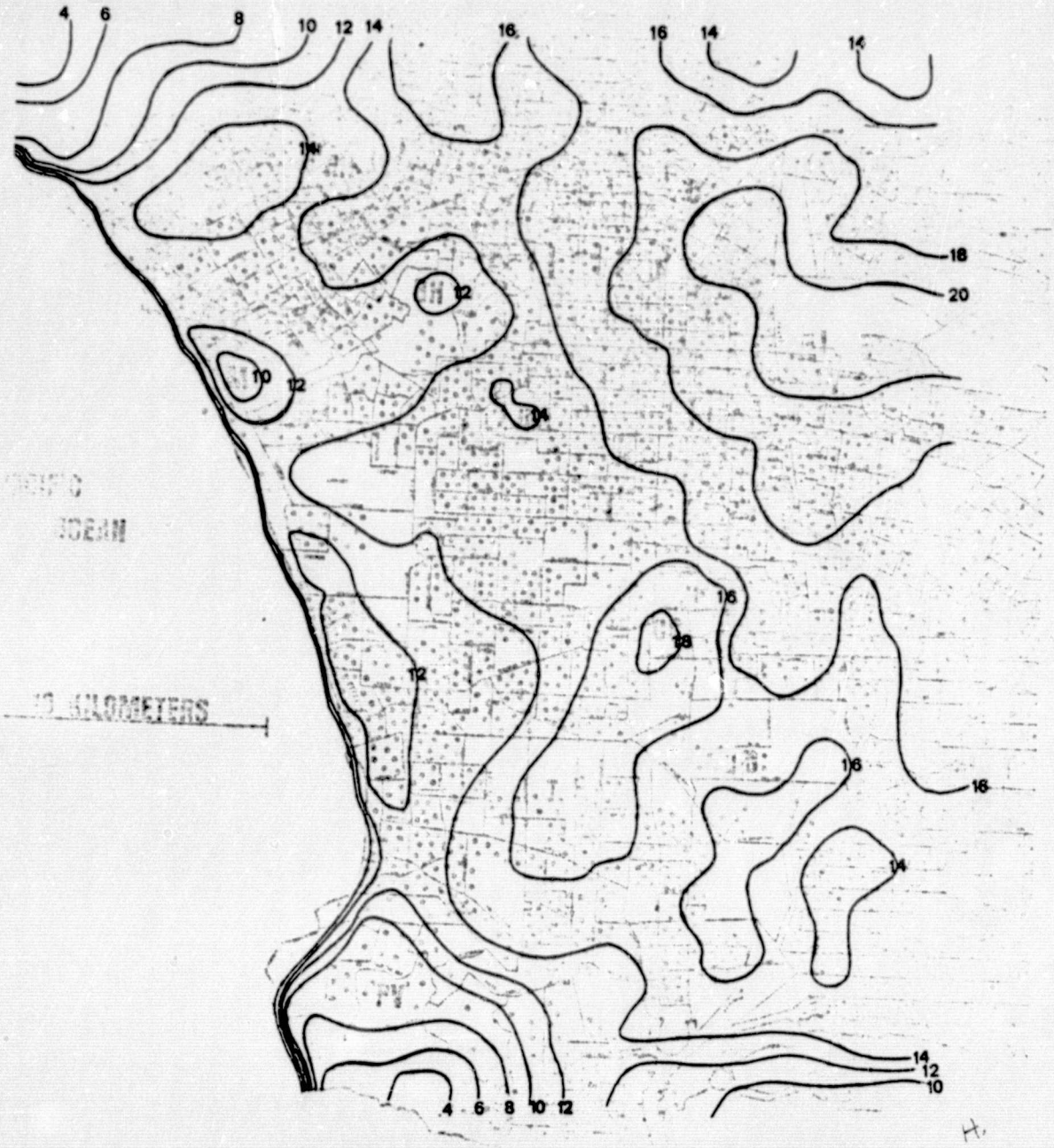

Figure 17. Los Angeles surface sensible heat flux (÷ 10) at 2:00 P.M. (R_N = 630 W/m^2).

extends inland and covers an area several kilometers square. As with the daytime temperatures, the coastline again corresponds to a sharp gradient in the pattern.

The most general feature is the increase in flux between the coastline and interior, reflecting the land use pattern in which suburban tracts congregate near the coast while heavy industry and commercial centers are located inland. Thus, a striking relationship between urbanization and large sensible heat flux is quite apparent in this figure.

3.2.6 May 31 Surface Evaporative Flux, E_o

The map of surface moisture flux, E_o, presented in Figure 18 exhibits a pattern which is closely related to the distribution of the sensible heat flux over the Los Angeles Basin. In general, areas which are minima of H_o appear as maxima of E_o and vice versa. The value of E_o has a marked minimum over the commercial-industrial districts near downtown Los Angeles (M,I) with the lowest isopleths surrounding two areas where E_o is below 237 w/m^2. The largest moisture fluxes occur over the high terrain (SM and PV), and over the grassy open areas where the moisture availability (Figure 15) was also found to be large. It is evident that the evaporation over sparsely vegetated regions is relatively small although E_o exhibits values which are as large as H_o in regions where the latter is a maximum.

3.3 St. Louis June 9 and 10, 1978

This case study uses data derived from a day-night pair of orbits, one on the morning of the ninth and another during the afternoon of the tenth. During this 36-hour period a high pressure ridge moved

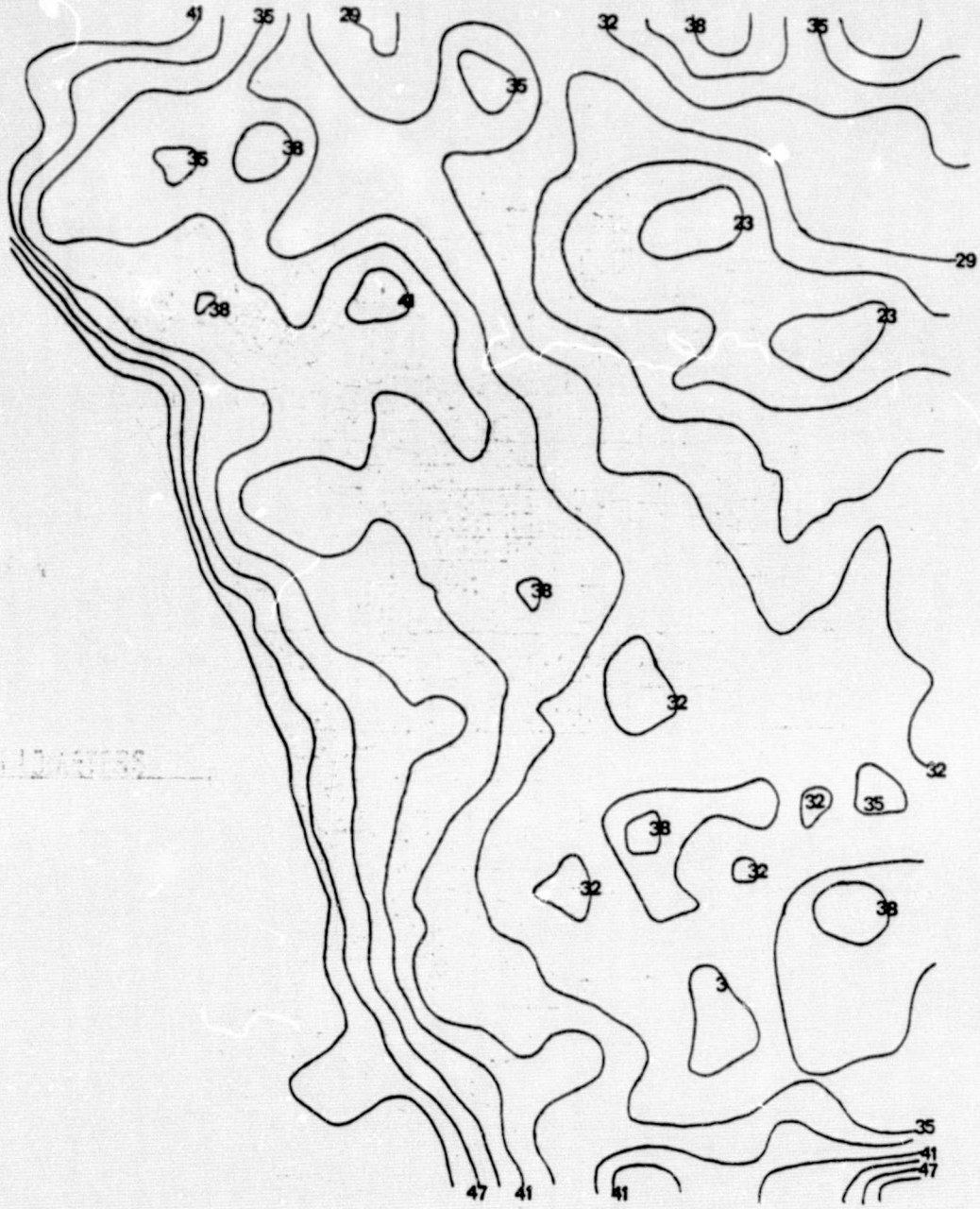

Figure 18. Los Angeles surface moisture flux (÷ 10) at 2:00 P.M. (R_N = 630 W/m^2).

eastward across the center of the country bringing fair weather and mild temperatures. Large-scale subsidence resulted in cloudless skies throughout the period with values of precipitable water less than one-half of an inch. The dry atmosphere resulted in only small water vapor corrections being applied to the satellite-derived black-body surface radiometric temperatures. Precipitation in the area had amounted to less than one-quarter inch over the four days prior to the satellite passes and therefore the ground surface was probably quite dry.

3.3.1 St. Louis Daytime Temperatures, T_D

The map of daytime temperature in Figure 19 displays a wide variation over the working area with values ranging from 23°C to above 32°C in city centers. The three urban sites which show the highest temperatures include downtown St. Louis (D), East St. Louis across the river (E), and the industrial center of Granite City (G). Metropolitan St. Louis is contained mostly within an area of approximately 25 km^2. In this region the ground temperatures vary from 32° to 34°C. Maximum temperatures are located near the City Hall and Memorial Plaza district where high-rise office buildings, parking lots, and a dense network of roads and highways compose an urban ground fabric with little vegetation. Both East St. Louis and Granite City are also completely urbanized with significant areas of heavy industry. Several other non-urban sites (identified by the letter C) possess daytime temperatures exceeding 30°C; all of these sites are separated from the urban centers by several kilometers and are located to the northwest, northeast, and southeast of the city. Examination of U.S. Geological Survey Land Use maps indicates that these areas consist

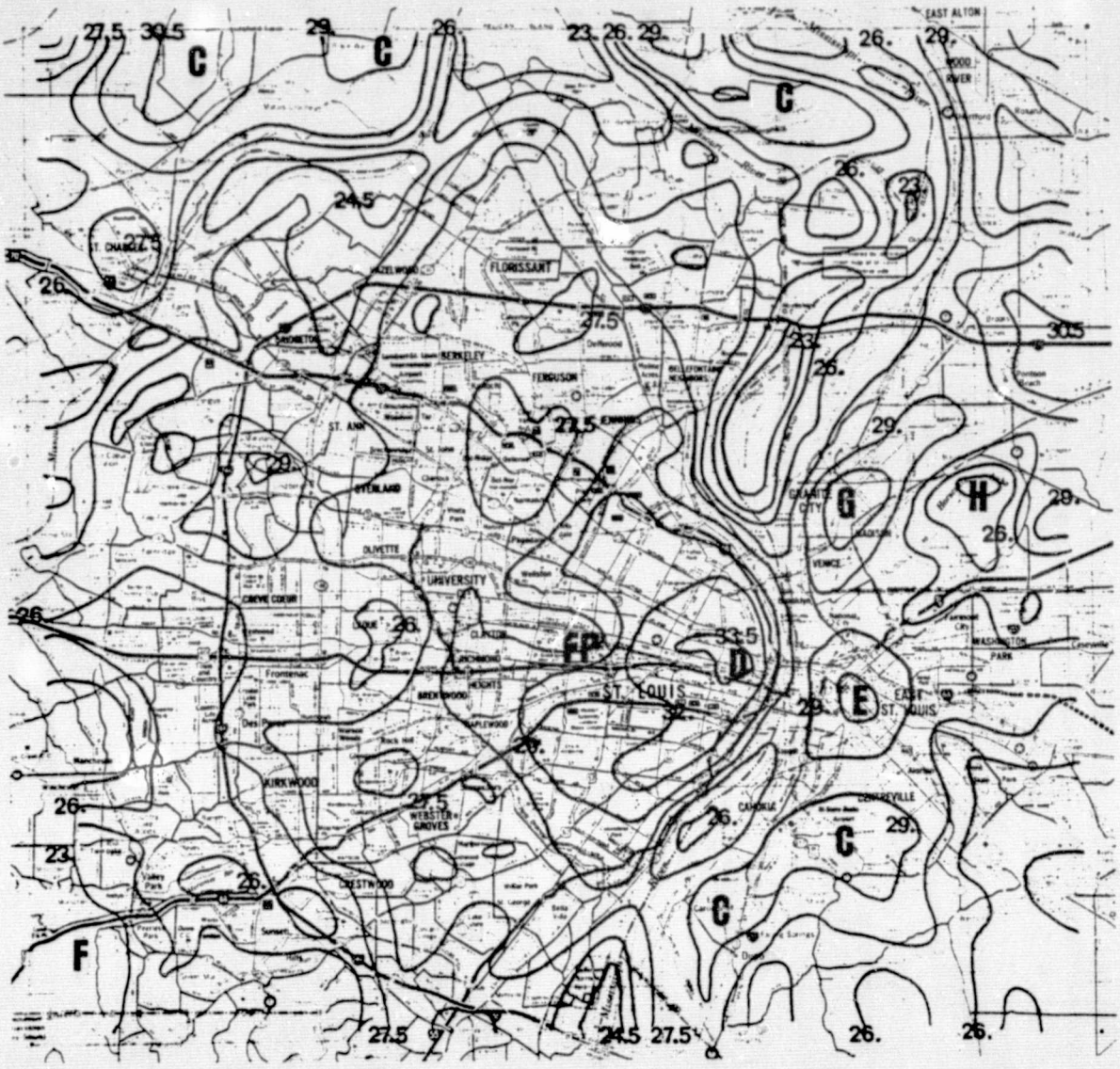

Figure 19. St. Louis, June 10, 1978 daytime surface temperature analysis.

of cropland and pasture characterized by extensive areas of open field and low vegetation.

The water bodies are all well-defined by isopleths of lower temperature with the lowest isotherm being 23°C. Although actual river and lake temperatures varied from 15° to 19°C in the raw measurements, the smoothing of the data combined with the elimination in the analysis of isotherms below a certain value tend to remove detail from the analysis around bodies of water such as the Mississippi River. The most evident ground temperature minima are centered in the southwest corner of the map (F) where a large expanse of deciduous trees remains despite the proximity of urbanization.

3.3.2 St. Louis Nighttime Temperatures, T_N

The nighttime range of temperature presented in Figure 20 reflects urban-rural differences which are much smaller than during the day with values between 3.5° and 6.5°C. The St. Louis urban center possesses the warmest temperatures. Over the downtown area near the river, values are above 6°C while a significant region surrounding this area exceeds 5.5°C. In comparison, typical rural temperatures vary from 4° to 5°C. The urban sites of East St. Louis (E) and Granite City (G), which were pronounced daytime maxima, do not display significant nighttime anomalies. Also, the cropland and pasture sites (C) which were daytime hotspots are actually nighttime minima, especially the areas to the northwest and northeast of the city where temperatures are below 4°. The rivers and Horseshoe Lake appear in the isotherm pattern as distinct temperature maxima in excess of 8°C, but the actual surface temperature pattern over the water is not delineated very well for reasons previously stated.

Figure 20. St. Louis, June 9, 1978 nighttime surface temperature analysis.

3.3.3 St. Louis Moisture Availability, M

The moisture availability plot shown in Figure 21 reflects the remarkable variability in M across the working area with values ranging from less than .2 over the downtown area to greater than .9 over the forested region southwest of the city. As would be expected, the rivers and Horseshoe Lake are well-delineated by large values of M although this is partly fortuitous because the model in its present form is designed to simulate the energy balance of a boundary layer with a solid substrate-atmosphere interface.

The most obvious feature in this figure is certainly the marked reduction in the evaporation potential over the city where a large area centered on the downtown district is enclosed by the .2 contour and is almost coincident with the same region defined by the 32°C contour on the daytime temperature map. East St. Louis (E) and Granite City (G) also appear as M minima. The lack of vegetation in these industrial-commercial sites is the obvious causal mechanism for the low evaporation. The other sites which display M values below .3 are the pasture-cropland (C) areas, discussed earlier, where the vegetation is sparse and cropped short, allowing for strong heating of the surface during the day.

The only pronounced maximum of M (apart from the rivers and lakes) coincides with the forested region (F) in the far southwestern corner of the map where the moisture availability locally exceeds .9. Thus, M has a wide variability across the domain and is inextricably related to the land use and particularly to the vegetation type. The average range of M was generally between .3 and .6.

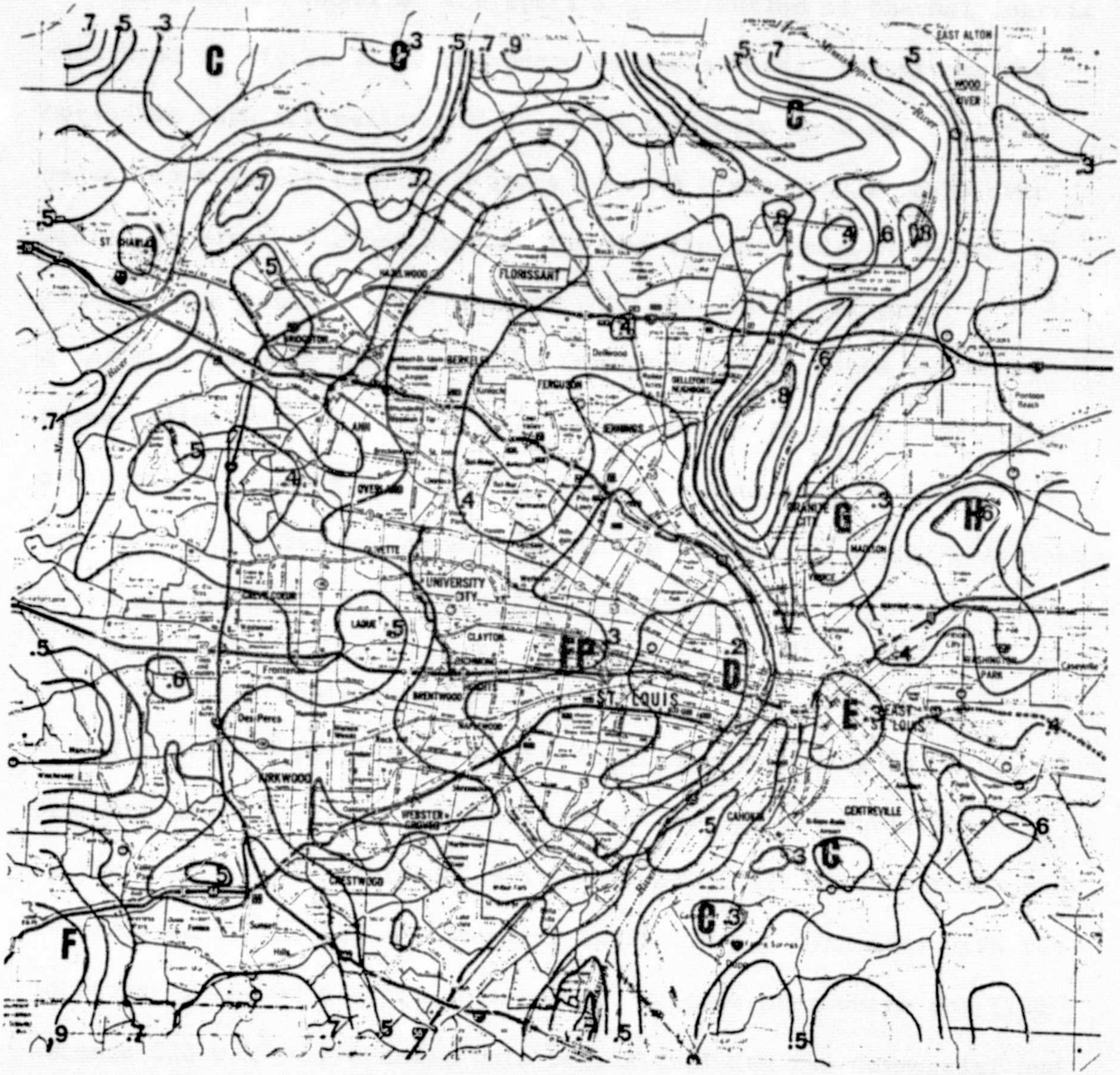

Figure 21. St. Louis moisture availability analysis.

3.3.4 St. Louis Thermal Inertia, P

As with Los Angeles, the spatial distribution of thermal inertia displayed in Figure 22 is unexpectedly indistinct. The rivers and Horseshoe Lake are delineated by sharp gradients in P and by large values over water; as with M the values of P are not reliable over bodies of water. Across most of the map the variation of P is minimal with values mostly between .025 and .035. The only disernible pattern appears at the cropland-pasture sites (C) where three minima of P below .025 are identifiable. Although these areas are quite hot during the day their relative inability to store that heat during the day and conduct it to the surface at night is typical of a surface fabric with low thermal inertia.

3.3.5 St. Louis Surface Heat Flux, H_o

The derived mapping of surface heat flux appearing in Figure 23 presents an intriguing representation of the spatial variation of H_o at the time of the afternoon orbit. The St. Louis metropolitan area is enclosed by the 251 w/m^2 contour which closely coincides with the location of the 32°C daytime isotherm. A large area where the flux exceeds 230 w/m^2 surrounding this region includes the commercial and industrial districts near the city center. The other urban sites of East. St. Louis (E) and Granite City (G) also reflect the significant alteration which urban substrates impose upon the energy balance compared to suburban or densely vegetated areas. The other maxima appear at the cropland sites which surround the suburbs of the city. The magnitude of H_o is as large at these locations as in the most built-up areas; indeed, the only isopleth where H_o exceeds 250 w/m^2 outside the city is centered over cropland just northeast of St. Louis. The typical range of H_o

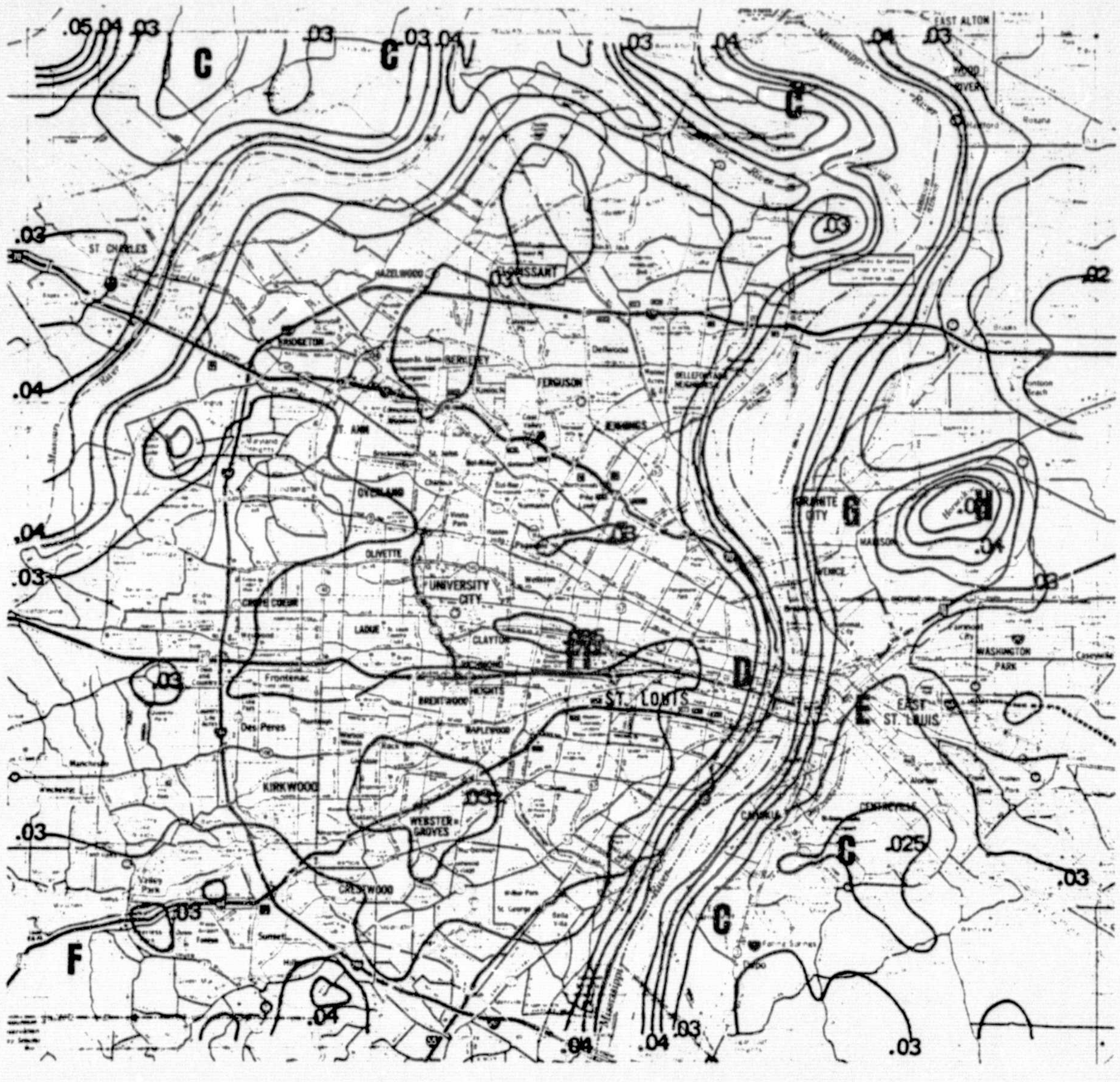

Figure 22. St. Louis thermal inertia analysis.

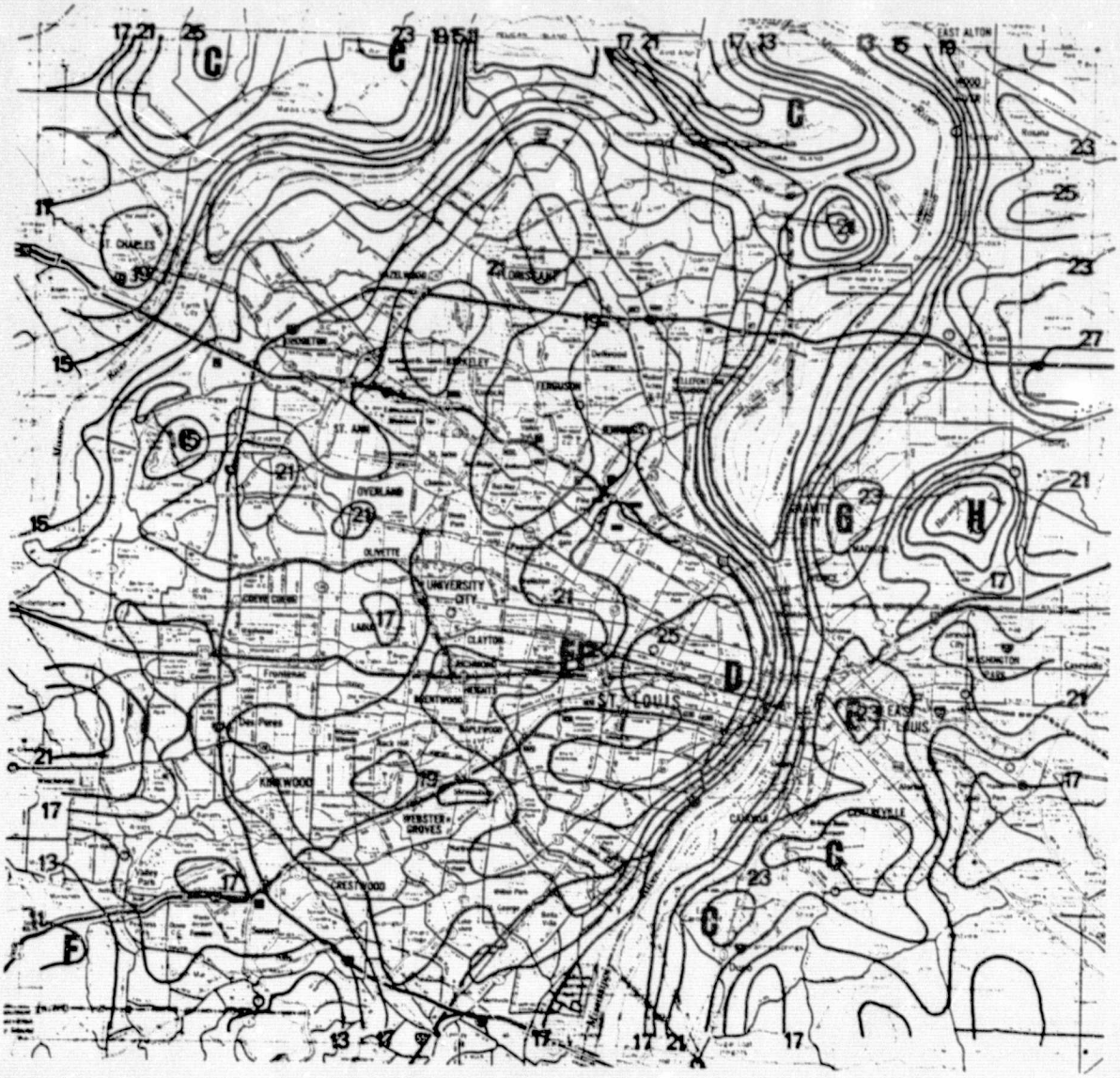

Figure 23. St. Louis surface sensible heat flux (÷ 10) at 2:00 P.M. (R_N = 640 W/m^2).

outside of the heavily urbanized areas is from 150 to 200 w/m^2 with the site of smallest heat flux located in the forested area southwest of the city where large evaporation by the plant canopy inhibits H_o.

3.3.6 St. Louis Evaporative Heat Flux, E_o

The map of surface moisture flux, E_o, shown in Figure 24 displays a distribution which closely corresponds to the fields of moisture availability and sensible heat flux shown in Figures 15 and 17. The downtown area (D) exhibits a strong minimum where an isopleth encloses a region over which E_o is below 265 w/m^2; this is the same area where M is smallest and H_o largest. The two other large urban sites (E,G) and the cropland-pasture areas (C) also appear as relative minima of E_o, reflecting the strong influence which vegetation exercises on the surface energy balance. The moisture flux is largest over the heavily forested area southwest of the city where E_o exceeds 500 w/m^2. Interestingly, as was the case with Los Angeles, the smallest values of E_o are larger than the maximum sensible heat flux.

3.4 Summary of Results

The maps of temperature, moisture availability, thermal inertia, and daytime heat and moisture flux across the areas centered on the cities of Los Angeles and St. Louis should aid in understanding the mechanisms responsible for the creation and maintenance of the urban heat island. The nature and magnitude of this anomaly is well-represented in the four plots of day and night temperatures. The daytime spatial variation is especially impressive with the city centers as much as 10°C warmer than nearby rural areas. Both St. Louis and Los Angeles exhibited well-defined maxima focused on the downtown, commercial and

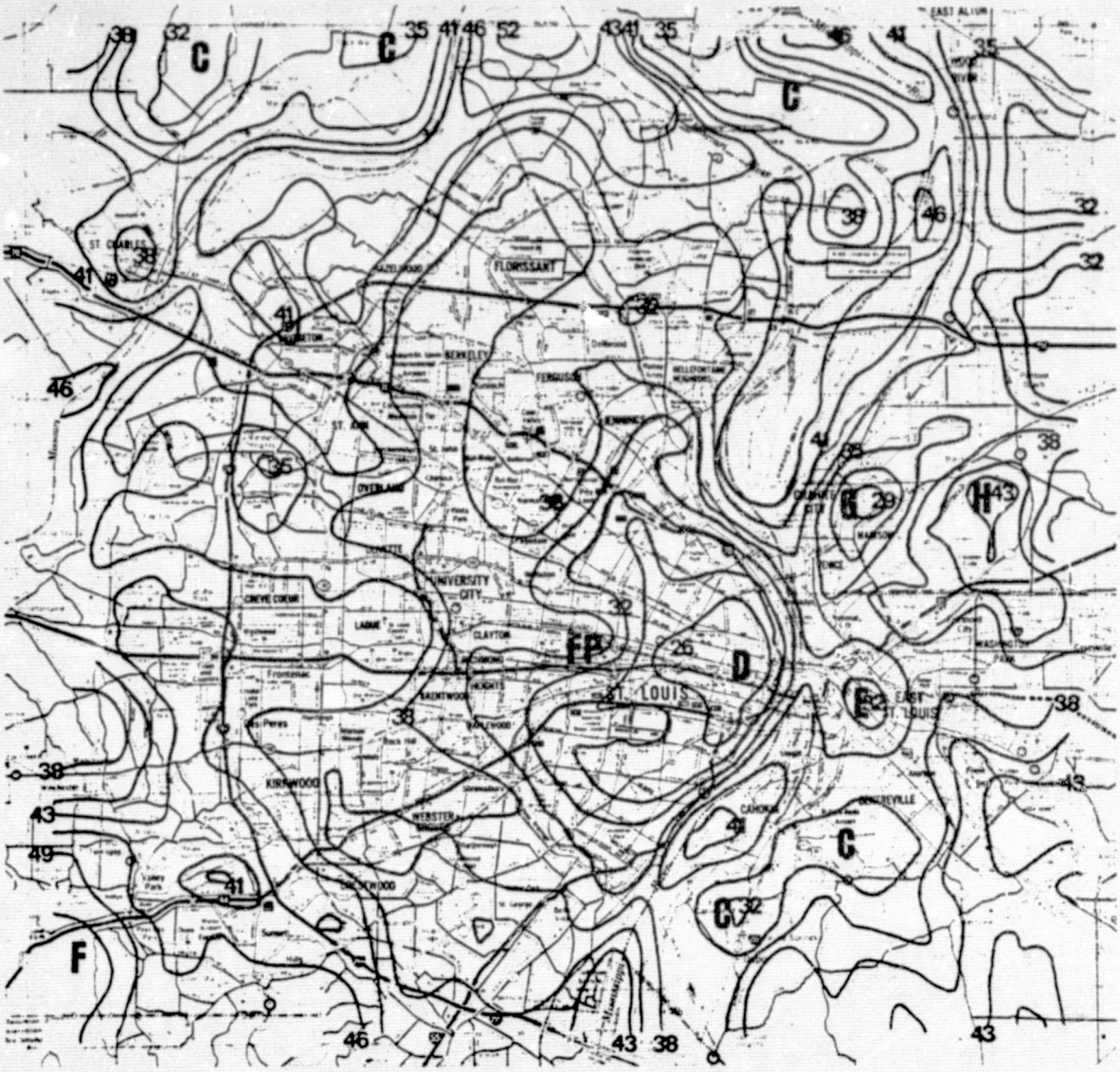

Figure 24. St. Louis surface moisture flux (÷ 10) at 2:00 P.M. (R_N = 640 W/m^2).

industrial districts near the civic centers reflecting the strong influence which land use plays in influencing the surface response to the solar forcing. Temperature minima consistently appear in locations with significant vegetation. Various grass-covered hilly areas scattered across the Los Angeles Basin and the forested region southwest of St. Louis all appear as sites where the surface temperature is distinctly lower than those over urban areas just a few kilometers away.

The patterns of moisture availability also show similarly clear variation with terrain, a reduction of M over urban and non-vegetated areas being the most obvious relationship. Over both St. Louis and Los Angeles these minima of M center directly on the down-town sites where commercial activity congregates and the urban fabric is a heterogeneous mixture of asphalt and concrete with few freely transpiring surfaces. The moisture budget over cities thus reflects excessive urban alteration of the substrate. Suburban regions consistently exhibit values of moisture availability between .3 and .5, values which seem to be typical for the overall region. The largest evaporation potential is found over grassy park areas in Los Angeles and the forested region southwest of St. Louis which had a moisture availability above .8, a value which seems reasonable over a completely vegetated site. The wide range of M values again reflects the profound effect that land cover variations have in producing the anamolies of urban microclimates.

The patterns of thermal inertia were more difficult to interpret. It was expected that P would show a wide variation across the working area with distinct maxima near the city centers reflecting the enhanced ability of urban substrate materials to store and conduct

heat. Both Los Angeles and St. Louis, however, failed to show any significant elevation of thermal inertia in the downtown districts. The only strong exception is a site southwest of Los Angeles where a local maxima of P is found. Since one- to four-story structures dominate this area, the land use would not seem to be significantly different from that in other high population density districts nearby. Therefore, it is not immediately apparent why the thermal inertia should be higher at this particular location. The only readily understandable feature in the pattern of P appears on the St. Louis map over the pasture-cropland sites surrounding the perimeter of the city where there was a clear pattern of anomalously low values of thermal inertia, implying that open areas of close cropped vegetation or bare soil store heat less efficiently than fully vegetated or urbanized surfaces.

Maps of the surface heat and moisture flux were the most interesting as these plots represent H_o and E_o very near the time of maximum flux within a diurnal cycle. As expected, the urban centers are the foci of H_o maxima where the heat flux is two to three times greater than over more vegetated areas nearby. Both St. Louis and Los Angeles exhibit local values of H_o in excess of 250 w/m^2 downtown while over densely vegetated areas H_o was below 100 w/m^2. More importantly, the urban anomaly is not confined to small areas a few blocks square, but encompasses significant regions of 25-50 km^2 surrounding the city centers where the heat flux was much larger than suburban and rural values. A glaring example of the scale of variation can be seen in an unsmoothed enlargement of the St. Louis downtown district (Fig. 25) where Forest Park (FP) is seen to have a heat flux roughly half that of the city center just a few kilometers away.

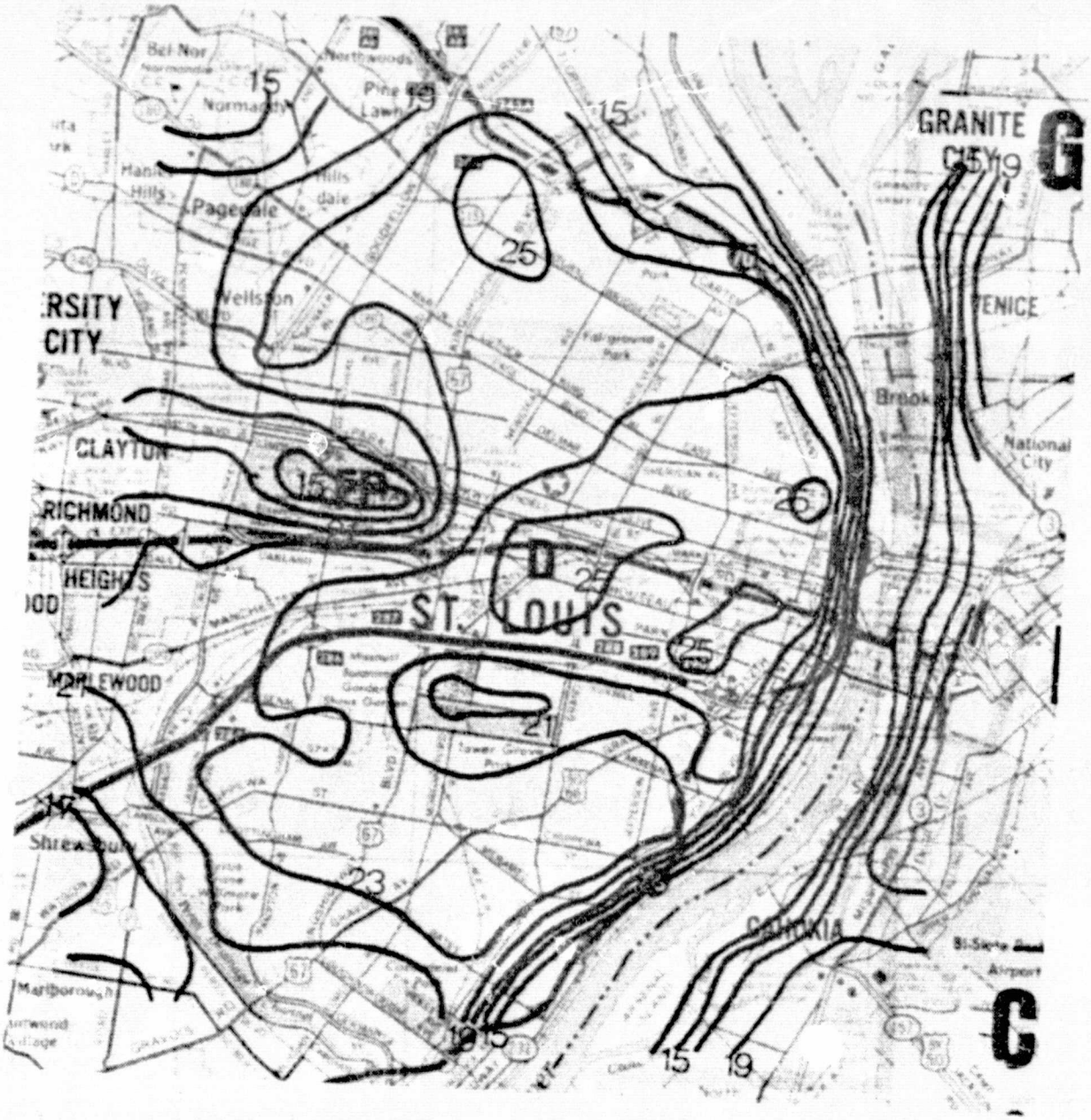

Figure 25. Enlargement of unsmoothed surface heat flux analysis over downtown St. Louis at 2:00 P.M.

Figures 26 and 27 display results from a model simulation which calculated the daytime evolution of the heat and moisture flux and net radiation over an urban and urral site, respectively, for the initial St. Louis conditions of June 9-10. It is evident that the low moisture availability (.175) in the urban simulation inhibits the evaporation and produces a large sensible heat flux whereas in the rural example (M=.5) the moisture flux is the most important term in the surface energy balance. Near solar noon (360 minutes) E_o is about 60% as large as the net radiation, R_N, for the rural case whereas in the urban example E_o is about 30% of R_N. Thus, it is evident that the energy balance at the surface must have a significant variation across an urban-rural canopy.

Figure 26. Daytime evolution of surface heat and moisture flux and net radiation from model simulation for St. Louis urban site (M = .175, P = .035).

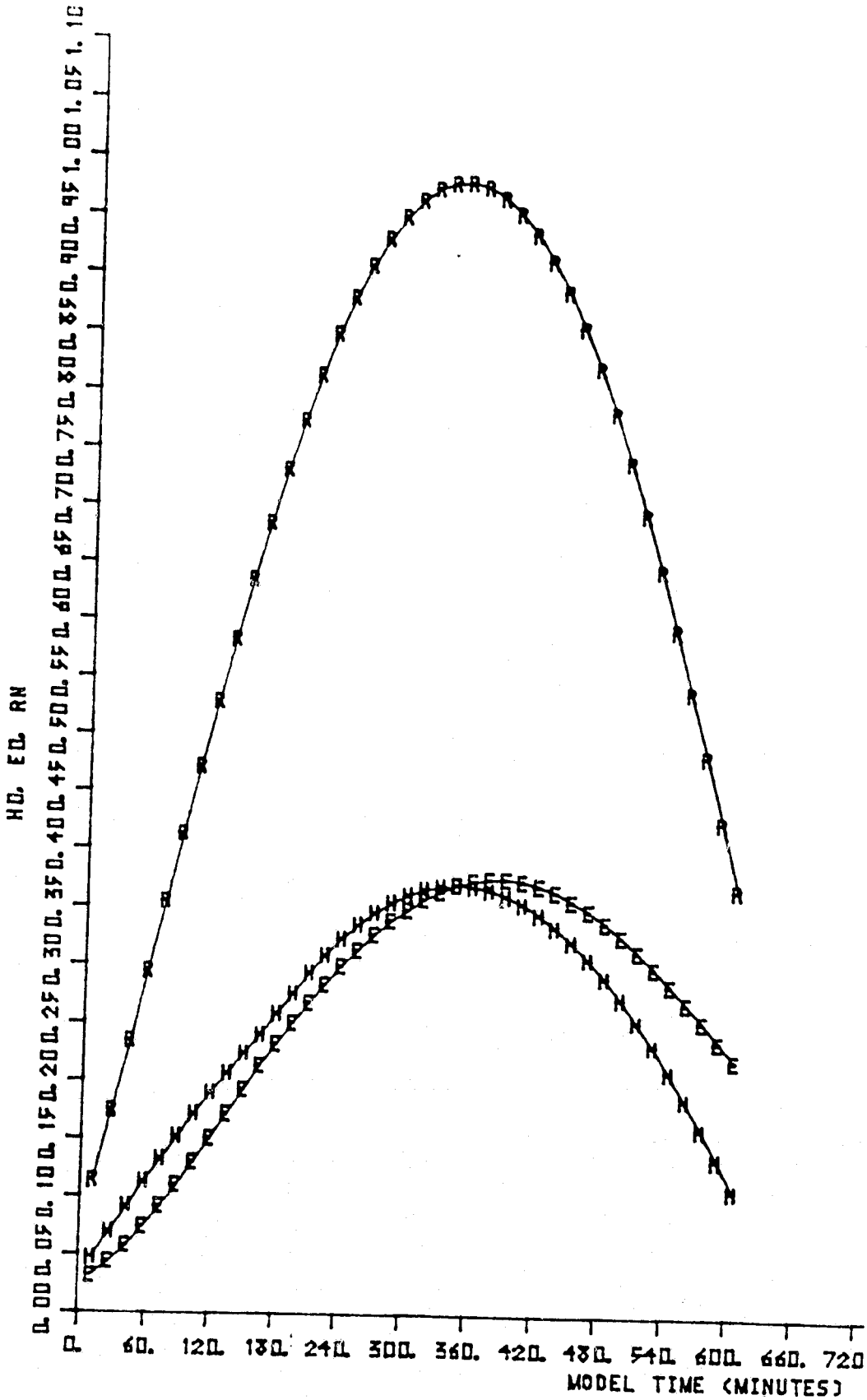
HG. EQ. RN
0.000 0.050 0.100 0.150 0.200 0.250 0.300 0.350 0.400 0.450 0.500 0.550 0.600 0.650 0.700 0.750 0.800 0.850 0.900 0.950 1.000 1.050 1.10
0. 60. 120. 180. 240. 300. 360. 420. 480. 540. 600. 660. 720
MODEL TIME (MINUTES)

Figure 27. Daytime evolution of surface heat and moisture flux and net radiation from model simulation for St. Louis rural site (M = .5, P = .035).

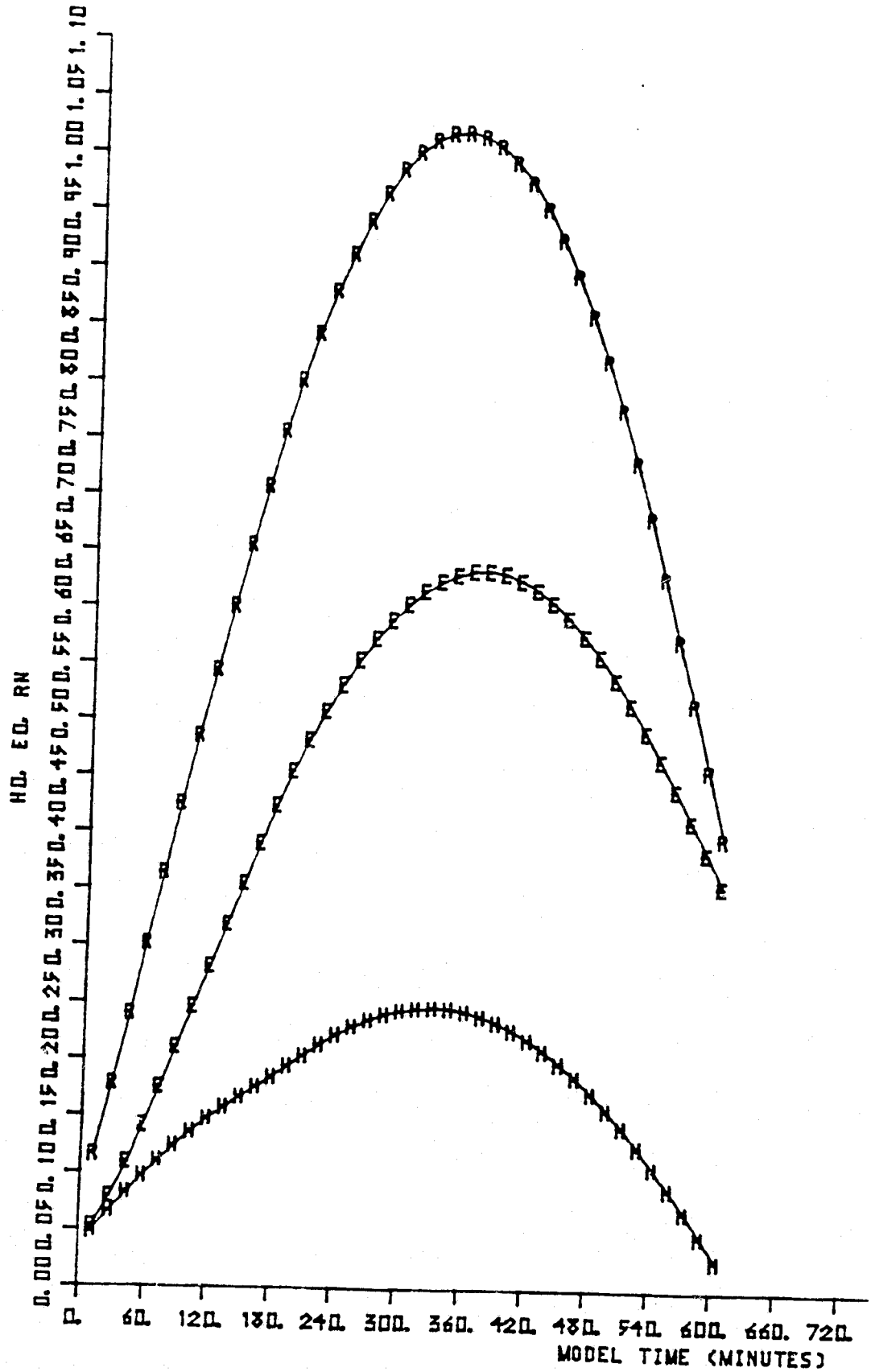
HO. EO. RN
0. 00 0. 05 0. 10 0. 15 0. 20 0. 25 0. 30 0. 35 0. 40 0. 45 0. 50 0. 55 0. 60 0. 65 0. 70 0. 75 0. 80 0. 85 0. 90 0. 95 1. 00 1. 05 1. 10
0. 60. 120. 180. 240. 300. 360. 420. 480. 540. 600. 660. 720.
MODEL TIME (MINUTES)

4. CONCLUSIONS AND SUGGESTIONS FOR FUTURE RESEARCH

A numerical procedure has been developed which uses satellite-derived surface temperature fields in combination with output from a numerical model of the boundary layer to infer the spatial distribution of the effective surface parameters, M and P, and the sensible and evaporative heat fluxes at the surface. The approach is general and may suitably be applied to any surface for which temperature data are available and over which horizontal homogeneity of large scale meteorological features may be assumed. The final result of the analysis is the mapping of the above quantities over the two urban areas examined in this research; Los Angeles and St. Louis. The plots presented represent a unique array of information which allows objective conclusions to be formulated concerning the mechanisms which produce and maintain the temperature anomaly in cities known as the urban heat island. Moreover, the maps of sensible and latent heat flux at the surface present for the first time the spatial representation of how the available radiation at the surface is partitioned according to the land use and vegetation cover.

Thermal inertia and moisture availability have been proposed as the two parameters which are most responsible for the temperature variations over a rural-urban complex (Carlson and Boland, 1978). The two case studies performed in the present research suggest that M is indeed the governing parameter during the day with both downtown areas appearing as distinct minima in M whereas suburban and rural areas possess much larger evaporation rates. The areas of daytime temperature maxima all correspond quite closely to minima in moisture availability. Conversely, the two plots of thermal inertia were

surprisingly ill-defined. It was anticipated that both Los Angeles and St. Louis would exhibit maxima in P, reflecting the enhanced ability of the urban substrate to store and conduct heat. Although both cities were relatively warm at night, P did not exhibit significant elevations in either location. The only exception is a small maximum in P centered approximately five miles southwest of downtown Los Angeles in a high population density residential area. This site is quite similar to numerous others within the Los Angeles Basin and the only hypothesis which may partly explain this anomaly is that the anthropogenic heat input (which has not been considered in the present form of the model) is relatively large over this location. This would suggest that the site is not a maximum of P but instead might actually possess significant values of anthropogenic heating with values of thermal inertia similar to those over the remainder of the Basin. In any case, it may be concluded that the nighttime temperature anomalies over both St. Louis and Los Angeles are not exclusively determined by large values of thermal inertia but are mainly the residual of the daytime anomalies produced by a larger heat storage due to a reduction in evaporation. This result is intriguing and differs from previous supposition concerning the distribution of P over an urban-rural canopy.

Clearly, any comprehensive study of urban microclimates should include an investigation of the anthropogenic heat input. Especially over cities at high latitude during the winter season, anthropogenic heat input may represent a significant fraction of the surface energy balance. In principle, if the thermal inertia can be assumed constant (or at least approximately so) across an urban basin, the same analysis

which was employed to solve for M and P might be used to infer M and the anthropogenic input, A_o. In general, any two terrain parameters may be determined from the analysis of day-night temperature pairs if all other parameters are known. In the future, the spatial variation of roughness length might be investigated but it is unlikely that present models possess the necessary accuracy to correctly infer effects of changes in roughness

The mapping of the sensible and evaporative heat fluxes at the surface have visibly demonstrated the alteration of the surface energy balance caused by cities. Both urban centers appear as distinct maxima of H_o and minima of E_o and these regions correspond very closely with the sites of highest daytime temperature. The variation of the surface heat flux undoubtedly has significant influence on the distribution of cloudiness and rainfall over and downwind of cities. During the convective precipitation season especially, the large heat flux over cities may act as a trigger mechanism for shower and thundershower activity.

The combination of modeling and remote sensing techniques described in this thesis holds promise for a variety of practical applications. The spatial variation of H_o could constitute an important input to mesoscale models for investigating the dynamic response of the atmosphere to urban and mesoscale variations in terrain parameters such as M and P which are presently only crudely estimated or entirely neglected in boundary layer components of large-scale models.

Operationally, the spatial variation of moisture availability could provide important information for use in agricultural and forest meteorology. For example, from an analysis of M it may be determined

if the moisture content of vegetation has reached the wilting point, the knowledge of which will aid in irrigation scheduling and also in the evaluation of forest fire threat. Also, determination of the time-integrated heat flux may supply useful information for diffusion models which employ mixed-layer scaling. Other uses, not yet foreseen, will undoubtedly emerge in the future.

REFERENCES

Atwater, M. A., 1972: Thermal changes induced by urbanization and pollutants. Preprints Conf. Urban Environment and Second Conf. on Biometeorology, Philadelphia, Amer. Meteor. Soc., 153-159.

_____, 1975: Thermal changes induced by urbanization and pollutants. J. Appl. Meteor., 14, 1061-1071.

Augustine, J., 1978: A Detailed Analysis of Urban Ground Temperature and Albedo Using High-Resolution Satellite Measurements, M.S. Thesis, Dept. of Meteorology, The Pennsylvania State University.

Benoit, R., 1977: On the integral of the surface layer profile-gradient functions. J. Appl. Meteor., 16, 859-861.

Blackadar, A. K., 1976: Modeling the nocturnal boundary layer. Third Symp. on Atmospheric Turbulence, Diffusion, and Air Quality, Rayleigh, N.C., 26-49, Oct. 19-22, 1976.

Boland, F. E., 1977: A Model for Determining Surface Temperatures and Sensible Heat Fluxes over the Urban-Rural Complex. M.S. Thesis, Dept. of Meteorology, The Pennsylvania State University.

Braham, R. R. and Wilson, D., 1977: Effects of St. Louis on convective cloud heights, J. Appl. Meteor., 17, 587-599.

Carlson, T. N., Augustine, J. A. and Boland, F. E., 1977: Potential application of satellite temperature measurements in the analyses of land use over urban areas. Bull. Amer. Meteor. Soc., 96, 91-114.

Carlson, T. N. and Boland, F. E., 1978: Analysis of urban-rural canopy using a surface heat flux/temperature model. J. Appl. Meteor., 17,

Chandler, T. J., 1965: The Climate of London. London, Hutchinson and Co., 292 pp.

Changnon, S. A., 1969: Recent studies of urban effects on precipitation in the United States. Bull. Amer. Meteor. Soc., 50, 411.

_____, 1978: Urban effects on severe local storms at St. Louis. J. Appl. Meteor., 17, 578-586.

Ching, J. K., Clarke, J. F. and Godowitch, J. M., 1978: Environmental Protection Agency, Research Triangle Park, N.C. 27711 (unpublished article).

REFERENCES (Continued)

Cogan, J. L. and Willand, J. H., 1974: Mapping the sea surface temperature by the NOAA-2 satellite. Prepared for the Environmental Prediction Research Facility, Naval Postgraduate School, Monterey, California 93940, by Environmental Research and Technology, Inc., 72 pp.

Dabberdt, W. F. and Davis, P. A., 1974: Determination of energetic characteristics of urban rural surfaces in the greater St. Louis area. EPA Contract Rep. No. 68-06-1015, Stanford Research Institute, 77 pp.

Duckworth, F. S. and Sandberg, J., 1954: The effect of cities upon horizontal and vertical temperature gradients. Bull. Amer. Meteor. Soc., 35, 198-207.

Estoque, M. A., 1963: A numerical model of the atmospheric boundary layer. J. Geophys. Res., 68, 1103-1113.

Howard, L., 1833: The Climate of London Deduced from Meteorological Observations Made in the Metropolis and at Various Places Around It., 2nd ed., 3 vols., London, J. and A. Arch.

Huff, F. A. and Vogel, J. L., 1978: Urban, topographic and diurnal effects on rainfall in the St. Louis region. J. Appl. Meteor., 17, 565-577.

Landsberg, H. E., 1956: The Climate of Towns in Man's Pole in Changing the Face of the Earth. Chicago, University of Chicago Press, 584-606.

Landsberg, H. E. and Maisel, T. N., 1972: Micrometeorological observations in an area of urban growth. Boundary-Layer Meteor., 2, 365-370.

Manual of Remote Sensing, 1975: American Society of Photogrammetry, Falls Church, Va., 867 pp.

Matson, M. et al., 1978: Satellite detection of urban heat isalnds, Mon. Wea. Rev., 106, 1725-1734.

Mellor, G. L. and Yamada, T., 1974: A hierarchy of turbulence closure models for planetary boundary layers, J. Atmos. Soc., 31, 1791-1806.

Montieth, J. L., 1961. An empirical method for estimating long-wave radiation exchanges in the British Isles. Quart. J. Roy. Meteor. Soc., 87, 171-179.

Myrup, L. O., 1969: A numerical model of the urban heat island. J. Appl. Meteor., 8, 908-918.

REFERENCES (Continued)

Nappo, C. J., 1972: A numerical study of the urban heat island. Preprints Conf. Urban Environment and Second Conf. on Biometeorology, Philadelphia, Amer. Meteor. Soc., 1-4.

_____, 1975: Parameterization of surface moisture and evaporation rate in a planetary boundary layer model. J. Appl. Meteor., 14, 289-296.

Oke, T. R., 1968: Some results of a pilot study of the urban climate of Montreal. Climat. Bull. (McGill Univ.), No. 3, 36.

Outcalt, S. I., 1972: The development and application of a simple digital surface-climate simulator. J. Appl. Meteor., 11, 629-636.

Panofsky, H. A., 1974: The atmospheric boundary layer below 150 meters. X8058, Ann. Rev. Fluid. Mech., 6, 147-177.

Rao, P. K., 1972: Remote sensing of urban heat islands from an environmental satellite. Bull. Amer. Meteor. Soc., 53, pp. 647-648.

Sasamori, T., 1970: A numerical study of atmospheric and soil boundary layers. J. Atmos. Sci., 27, 1122-1137.

Sellers, W. D., 1965: Physical Climatology. The University of Chicago Press, Chicago, 272 pp.

Tag, P. M., 1968: Surface Temperatures in an Urban Atmosphere, Part I, Rep. 15, NSF Grant GA-3956, The Pennsylvania State University.

Tennekes, H., 1970: Free convection in the turbulent Ekman layer of the atmosphere. J. Atmos. Sci., 27, 1027-1034.

_____, 1973: A model for the dynamics of the inversion above a convective boundary layer. J. Atmos. Sci., 30, 558-567.

Vigeant, S. A., 1978: Comparative Verification of Two Atmospheric Boundary Layer Models. M.S. Thesis, Dept. of Meteorology, The Pennsylvania State University.

Yap, D. H. and Oke, T. R., 1974: Sensible heat fluxes over an urban area--Vancouver, B.C. J. Appl. Meteor., 13, 880-890.

Zdunkowski, W. G. and Trask, D. C., 1971: Application of a radiative-conductive model to the simulation of nocturnal temperature changes over different soil types. J. Appl. Meteor., 10, 937-946.